Diffusion of the Tracers Cu^{67}, Ni^{66}, and Zn^{65} in Copper-Rich Solid Solutions in the System Cu-Ni-Zn

K. J. ANUSAVICE AND R. T. DeHOFF

Tracer diffusion coefficients were determined for the three isotopes, Zn^{65}, Cu^{67}, and Ni^{66}, in homogeneous Cu-Ni-Zn binary and ternary alloys, to 30 pct Ni and Zn, and pure copper as a function of composition and as a function of temperature, within about 250°C of the solidus surface. Activation energies and D_0 factors were determined as functions of composition from these measurements. It is found that as the composition plane is traversed in the general direction from high nickel compositions on the copper-nickel binary to high zinc concentrations on the copper-zinc binary, *i.e.*, as nickel is replaced by zinc, the diffusivity of all three tracers increases, and the activation energy for diffusion decreases. The total change in diffusivity across the composition plane is about two orders of magnitude. The three diffusivities are always in the order: $D^*_{Zn} > D^*_{Cu} > D^*_{Ni}$, with the ratio being 9:3:1 at 900°C for all compositions. The three activation energies are usually in the order $Q^*_{Ni} > Q^*_{Cu} > Q^*_{Zn}$. These results are shown to be consistent with atom size and electron-to-atom concentrations of the three species in this alloy system.

A long-range experimental program at the University of Florida on the complete analysis of diffusion behavior in a single ternary system has concentrated upon the fcc solid solution in the system Cu-Ni-Zn. The objectives of this program are: 1) to provide the experimental information which is necessary for assessing the validity and utility of various approaches to the theoretical phenomenological description of multicomponent diffusion in solid solutions;[1-5] and 2) to provide a real basis for physical insight into the ways in which atomic species interpenetrate to establish diffusion paths for a system. The initial phase of this study focused upon the penetration behavior of the three tracers, Cu^{67}, Ni^{66}, and Zn^{65} in homogeneous copper-rich alloys containing up to 30 pct Ni and Zn. Tracer diffusion coefficients of Zn^{65} have been reported earlier;[6] the present paper is a final report on the tracer diffusion behavior of all three isotopes in this system. Interdiffusion behavior, and its relation to the tracer diffusion coefficients, will be reported in a subsequent paper.

The approach applied to the present experimental study involves electroplating the tracer upon an appropriate, polycrystalline, homogeneous alloy, subjecting the sample to a diffusion anneal, and then determining the penetration by the standard lathe-sectioning technique. The experimental procedure is divided into the following subject areas: 1) alloy preparation; 2) density determination; 3) diffusion sample preparation; 4) the diffusion anneal; 5) lathe-sectioning and activity analysis; and 6) data processing. The experimental results are reported as: 1) typical penetration curves; 2) variation of diffusivities with concentration; 3) temperature dependence of the diffusion coefficients; 4) empirical correlations of tracer diffusivities and activation energies with composition. The results are then shown to be consistent with the compositional variation of atom sizes and electron-to-atom ratios for this system.

K. J. ANUSAVICE, formerly Graduate Student, Department of Materials Engineering, University of Florida, Gainesville, Fla., is presently with the U. S. Atomic Energy Commission, Aiken, S. C. R. T. DeHOFF is Professor, Department of Metallurgical and Materials Engineering, University of Florida.

Manuscript submitted October 1, 1971.

EXPERIMENTAL PROCEDURES

Alloy Preparation

Two series of binary and ternary Cu-Ni-Zn alloys were prepared for the tracer studies. The first set of alloys was produced in our laboratories, and was used in the tracer diffusion investigations involving Zn^{65}. The compositions of the base materials used in preparing these alloys are given in Table I. Alloys used for the Ni^{66} and Cu^{67} tracer experiments were purchased from Materials Research Corporation. Nominal compositions of these alloys were at intervals of 10 at. pct in the composition field. To facilitate discussion, each alloy was given a two digit designation, with the first digit indicating the nickel content, and the second the zinc content. Thus, 03 represents a 0 pct Ni, 30 pct Zn, balance copper alloy; 31 represents 30 pct Ni, 10 pct Zn, balance copper alloy; and so on. Nominal and actual compositions of the alloys used in this study are presented in Table II. Alloys purchased from Materials Research Corporation are designated with superscript (+).

No attempt was made to prepare single crystals of these alloys, although it is recognized that distortions of the penetration profiles may result from the presence of grain boundaries.[7,8] After homogenization, the samples used in this study were large-grained (of the order of 1 to 3 mm), and by confining the study to within 250°C of the solidus temperature, the problems associated with diffusion short-circuiting paths were largely eliminated.

The first series of alloys were induction melted in evacuated, sealed Vycor capsules. The capsule had a hot-top configuration, in order to minimize shrinkage pipe during solidification. The molten alloys were water quenched to minimize segregation. The $\frac{1}{2}$ in. ingots were swaged to approximately $\frac{3}{8}$ in. diam rods,

Table I. Compositions of Base Materials Used in This Study (Compositions Listed are Given in Weight Percent)

Cu:	99.999	Cu ($\frac{3}{4}$ in. diam by 12 in. long bar) Purchased through Materials Research Corporation (MRC)
	99.99	Cu ($\frac{1}{4}$ by 2 by 12 in. electrode sheet) Courtesy of American Smelting and Refining Company
	99.95	Cu ($\frac{5}{8}$ in. sq by 4 in. long ingot) Courtesy of Anaconda American Brass Company
Ni:	99.9	Ni
	0.003	Cu
	0.030	Fe
	0.004	S
	0.060	C
	Trace	Si and Co
Zn:	99.9951	Zn
	0.0025	Pb
	0.0014	Cd
	0.0007	Fe
	0.0001	Cu
	0.0002	Ag
Muntz Metal:	60.85	Cu
	39.12	Zn (6 in. by 8 by 0.050 in. sheet) Cour-
	0.01	Pb tesy of Anaconda American Brass
	0.02	Fe Company
Cu-Ni Master Alloy:	63.5	Ni (4 in. sq by 10 in. long ingot) Cour-
	36.5	Cu tesy of International Nickel Company, Incorporated
Commercial Alloys:	Alloy 220	
	89.96	Cu
	10.03	Zn
	<0.01	Pb
	<0.01	Fe ($\frac{1}{2}$ in. diam by 36 in. long bar) Courtesy of Anaconda American Brass Company
	Alloy 240	
	79.60	Cu
	20.39	Zn
	<0.01	Pb
	<0.01	Fe

and homogenized within 30° to 50°C of the solidus temperature in evacuated quartz tubes. The homogenization time and temperature was adjusted according to the composition of the alloy, and selected alloys were spot-checked for chemical homogeneity.

The alloys supplied by Materials Research Corporation were arc melted in vacuum (for low zinc compositions) or in inert atmosphere (for high zinc compositions), and their compositions determined by wet chemical analysis. The homogenization treatments were essentially identical to those used for the first series of alloys.

Density Determination

In the lathe-sectioning technique, it is necessary to determine the thickness of each layer removed. This is done by collecting the chips as they are machined and weighing them on a microbalance. In order to convert the weight to the thickness of the slice removed, it is necessary to know the density of the alloy being machined. Accordingly, a small sample of each alloy was cut from the homogenized bar, and used to determine its density by the standard water immersion technique. The sample was turned to a cylinder and faced, notched at one end, cleaned, and dried thoroughly. It was weighed on a Mettler semi-microbalance, then suspended on a fine copper wire in a beaker of distilled water, and weighed in water. Corrections for the weight of the wire, and for the variation of the water temperature were included in the calculation of the density. The densities of the alloys used in this study are listed in Table II.

Table II. Densities of Cu-Ni-Zn Alloys

Alloy Designation	Composition, At. Pct Cu	Ni	Zn	Density, g/cm^3
00	99.99	–	–	8.96
01	88.9	–	10.1	8.80
02	79.5	–	20.5	8.67
03	69.8	–	30.2	8.53
10	90.7	9.3	–	8.95
11	80.4	9.3	10.3	8.79
12	70.2	9.3	20.5	8.68
13	60.1	9.1	30.8	8.57
20	81.8	18.2	–	8.95
21	70.8	18.8	10.4	8.80
22	60.6	18.6	20.8	8.69
23	50.3	18.7	31.0	8.60
30	71.4	28.6	–	8.94
31	61.2	28.2	10.6	8.79
32	50.8	28.2	21.0	8.72
33	40.7	27.9	31.4	8.64
00*	99.999	–	–	8.96
01*	90.25	–	9.75	8.82
02*	80.08	–	19.92	8.68
03*	70.94	–	29.06	8.55
10*	90.08	9.92	–	8.95
11*	82.72	12.55	4.73	8.88
12*	72.04	11.21	16.75	8.73
13*	65.06	10.82	24.12	8.64
20*	80.28	19.72	–	8.95
21*	69.68	19.42	10.90	8.81
22*	63.95	20.80	15.25	8.75
23*	55.17	20.59	24.24	8.66
30*	71.73	28.27	–	8.95
31*	60.97	29.49	9.54	8.81
32*	47.12	33.08	19.80	8.75
33*	40.30	30.70	29.00	8.68

Preparation of the Diffusion Samples

MACHINING AND POLISHING

Samples about $\frac{3}{4}$ in. long were cut from the homogenized bars, mounted in a precision lathe with an adjustable chuck[9] and faced perpendicular to the axis of the cylinder to within 0.0001 in. The face to be electroplated with tracer was hand ground through 4/0 paper, and an optical flat used to check the flatness of the surface. Specimens with surface irregularities greater than 0.0001 in. were repolished.

ELECTROPLATING

The polished end was cleaned in 95 pct ethanol just prior to electroplating. A thin layer of tracer was deposited from a mixture consisting of about 4 ml of tracer solution and a suitable electrolyte. The sample was placed in a holder and lowered to make contact with the solution, then withdrawn slightly so that a

Table III. Electroplating Conditions

Tracer	Zn^{65}	Ni^{66}	Cu^{67}
Tracer Solution	$ZnCl_2$ in HCl	$NiCl_2$ in HCl	$Cu(NO_3)_2$ in HNO_3
Electrolyte Composition	$AlCl_3$(12.5)	$NiSO_4$(20) $NiCl_2$(3)	$CuSO_4$(10) Na_2CO_3(30)
gpl H_2O	Na_2SO_4(47.5)	NH_4Cl(10) H_3BO_3(10)	KCN(15)
Bath Temperature, °C	~25	~25	~35
Plating Current Density, ma/cm^2	30	30	50
Plating Time, min	8-12	12-20	6-10

Table IV. Radiation Characteristics of Available Zn, Ni, and Cu Radioisotopes

Tracer	Half-Life	Principal Radiation	Energy of Radiation	
			β, MeV	γ, Mev
Zn^{65}	245d	γ, EC, β^+	0.33	1.11, 1.35
Ni^{63}	92y	β^-	0.067	–
Ni^{66}	55h	β^-, EC	0.20	0.20
Cu^{66}*	5.1m	β^-, γ	0.57, 0.66	1.038
Cu^{64}	12.8h	β^+, EC	0.57, 0.66	1.34
Cu^{67}	61h	β^-, γ	0.40, 0.48, 0.58	0.182, 0.090, 0.092

*See decay scheme of Ni^{66} in following section.

short column of solution was suspended from the polished face by capillary action. Current was supplied by a dry cell, and controlled by a variable resistor. Plating conditions were selected to produce a layer of the order of 0.1 μ in thickness, and a minimum activity of approximately 50 μCi. The plating conditions for each isotope, and the compositions of the electrolytes used, are listed in Table III.

ISOTOPE SELECTION

The radiation characteristics of the available Zn, Ni, and Cu isotopes which may be applied to tracer diffusion studies are listed in Table IV. The isotopes that were used, Cu^{67}, Ni^{66}, and Zn^{65}, were selected on the basis of half life and ease of detection. These isotopes were obtained from the Oak Ridge National Laboratory. The isotopes Cu^{67} and Ni^{66} are not commonly available, and were specially produced for this project through the cooperation of Dr. J. J. Pinajian and the Isotopes Development Center.[10] The copper isotope has a half life that is longer than that of Cu^{64}, which has been commonly used in diffusion studies. Ni^{63}, commonly used in tracer studies, is an emitter of weak β radiation; by using Ni^{66}, which is a γ emitter, in the present study, the necessity for acquiring the involved techniques necessary for measuring β activities was avoided.

The Diffusion Anneal

Because the experimental program spanned such a long period of time, a variety of furnaces and furnace control equipment was used for the diffusion anneals. Temperatures were measured by thermocouples calibrated against a National Bureau of Standards Pt/Pt-10 pct Rh standard couple. Temperatures were controlled by on-off controllers for low temperature, long time anneals, and by proportional, rate, reset controllers for high temperature, short time treatments. The hot zone temperature was regulated to within ±0.5°C for the proportional-type controllers, and to ±2°C for the on-off controllers. Specimens experiencing temperature variations of greater than ±2°C were rejected. Diffusion anneal times were estimated by applying the rule of thumb that $4\sqrt{D^*t}$ should be about 15 mils, where D^* is an approximate estimate of the tracer diffusion coefficient for the sample. This depth of penetration produced about 15 to 30 sections of measurable activity using the subsequent lathe-sectioning procedure.

Individual specimens, with tracer plated on one end, were placed in evacuated Vycor capsules, and inserted into the furnace at a predetermined temperature and time. Heating and cooling corrections were made at the end of the annealing period. Early in the investigation it was found that the zinc tracer evaporated essentially instantaneously, so that the entire specimen was subject to a uniform vapor pressure of radioactive zinc. This effect was examined both theoretically and experimentally, with the conclusion that this change in boundary conditions introduces no significant error into the application of the standard thin film solution.[11]

Lathe Sectioning and Activity Analysis

The analysis of the tracer penetration in the annealed samples requires the careful separation of thin layers of material from the plated end of the sample on a precision lathe. The resulting chips are carefully collected and weighed to determine the thickness of each layer as it is removed. The level of radiation in the chips from each layer is then measured with an appropriate counting device, and is proportional to the concentration of tracer solute present in the layer. Application of the thin film solution[12] to the resulting data on the penetration of the tracer allows the calculation of the tracer diffusivity for the sample. This procedure may be applied to systems in which tracer diffusion coefficients fall within the range 10^{-8} to 10^{-13} cm^2/sec. All diffusivities determined in the present study fall within this range.

Examination of the plated end of a sample after the diffusion anneal usually revealed small scale surface rumpling. This roughening was generally of the order of 0.0002 in., and in the worst case was 0.0005 in. A very light polish on 4/0 paper, until continuity of the polishing scratches was observed, reduced this rumpling to 0.0001 in. or less, as determined with an optical flat.

In order to insure that the penetration analyzed was essentially one dimensional (*i.e.*, to remove the effects of radial diffusional flow) a radial layer approximately $6\sqrt{D^*t}$ deep and $\frac{1}{8}$ in. wide was removed from the sample. The diameter after machining was measured with a vernier micrometer to within 0.0001 in.

The sample was then inserted into the adjustable chuck, which permitted adjustments of the orientation of the axis of the sample. Alignment was achieved with the help of a dial indicator with a working accuracy of 0.0001 in. Three fixed points on the circumference of the active surface were used as reference points, and the chuck adjusted until these three points agreed to

within 0.0001 in., and then locked in place. Material layers approximately 1 mil in thickness were then removed, starting at the active face, and the chips collected in a "Lucite" container surrounding the sample. The chips from each cut were then transferred to a preweighed thin-walled Pyrex culture tube and weighed on a semimicroanalytical balance. The weight of the chips was determined by difference; the volume was then calculated from the density measurements, and the thickness of the corresponding wafer calculated with the aid of the diameter measurement. The absorption of radiation in the walls of these Pyrex containers was established to be negligible for the isotopes used in this study.

The relative activities of the tracer in the chips from each layer were determined by standard counting procedures using a scintillation detector and pulse height analyzer. All samples were counted for a minimum of 10,000 counts. Suitable calibration standards were used for each isotope, and instrument stability was checked periodically during counting by referring to standard activities. Corrections for instrument dead times, isotope decay, and radiation absorption were found to be negligible for the selected counting rates, counting times, and sample geometry, respectively.

Data Processing

Measured values of the activity were plotted on a logarithmic scale vs the square of the penetration depth. According to the standard thin film solution for diffusion, if volume diffusion is dominant, such a plot should be linear, with a slope equal to $-\frac{1}{4}D^*t$. This behavior was found to hold over the full range of compositions used in this study for the three tracers. In a few cases, the "near surface effect"[13,14] was observed at one end of the plot, and at the other end, at low temperatures, deviations from linearity, normally associated with short circuiting mechanisms,[7,8] were also found. However, even in these cases, intermediate regions of the penetration plots were linear and permitted the evaluation of a diffusion coefficient from the standard thin film solution. Diffusivities were calculated by the method of least squares; confidence limits for each diffusivity were also evaluated.

Plots of the logarithm of the measured diffusivity vs the reciprocal of absolute temperature were obtained for each composition and tracer. All plots were linear with a high degree of correlation. Activation energies were calculated using the slope of these least square plots, confidence limits on the estimated activation energies were also determined.

A nonlinear least squares analysis was performed by computer[15] to develop an empirical correlation between the measured D^* values and concentration at 900°C. The same program was also applied to develop correlations between the activation energies (determined from the Arrhenius plots) and composition. These correlations, as well as the individual determinations of the diffusion coefficients and activation energies, are presented in the next section.

EXPERIMENTAL RESULTS

A total of sixteen nominal compositions, including pure copper, six binary alloys, and nine ternary alloys, were examined in the course of this work. A total of 381 diffusion coefficients were determined in the course of the program. These data were analyzed to yield 48 activation energies.

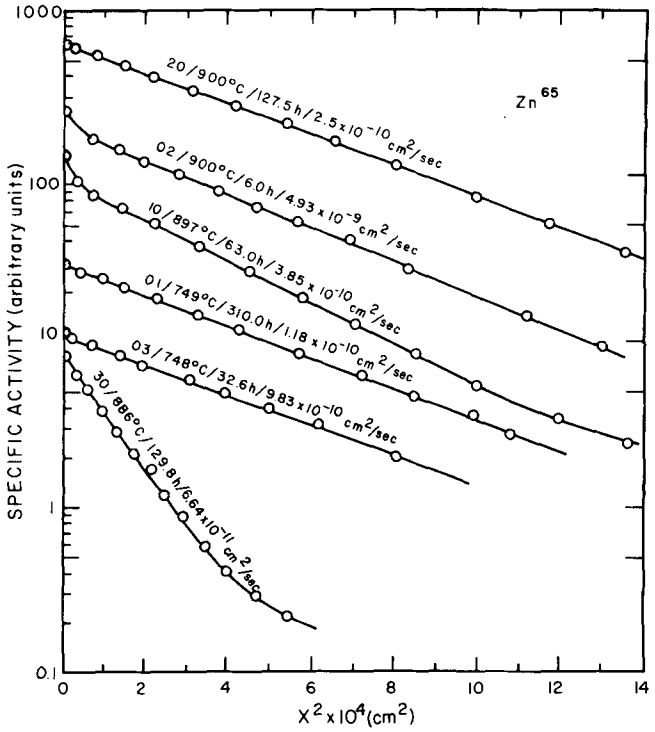

Fig. 1—Representative penetration plots for the diffusion of Zn^{65} in Cu-Ni and Cu-Zn alloys.

Penetration Plots and Measured Diffusivities

Typical penetration plots obtained for each of the tracers are given in Figs. 1 to 6. Information given on each curve includes the nominal composition, diffusion anneal temperature, and time, and the value of the diffusion coefficient determined from the plot. Specific cases illustrating the incidence of near surface and short circuiting effects are presented in these plots. The diffusivities determined from these and similar plots are presented in Tables V (Zn^{65}), VI (Cu^{67}), and VII (Ni^{66}). The alloy composition, diffusion anneal temperatures, and times corresponding to these diffusivities are also listed. For the Zn^{65} tracer, annealing temperatures ranged from 700° to 1080°C; annealing times ranged from 3 hr to 378.8 hr. For the Cu^{67} tracer, temperatures ranged from 720° to 1113°C, and times from 4 to 176.3 hr. Measurements of the Ni^{66} tracer diffusivities were made in the range 739° to 1134°C for periods of 3.7 to 547 hr.

Concentration Dependence of the Measured Diffusivities

The variation of the tracer diffusion coefficients for each of the isotopes with composition on the Gibbs triangle is graphically presented in the plots presented in this section. The 900°C isotherm was chosen for this display because diffusivities of all three isotopes could be determined over the full range of compositions covered in this study.

Figs. 7, 8, and 9 present isodiffusivity contours for

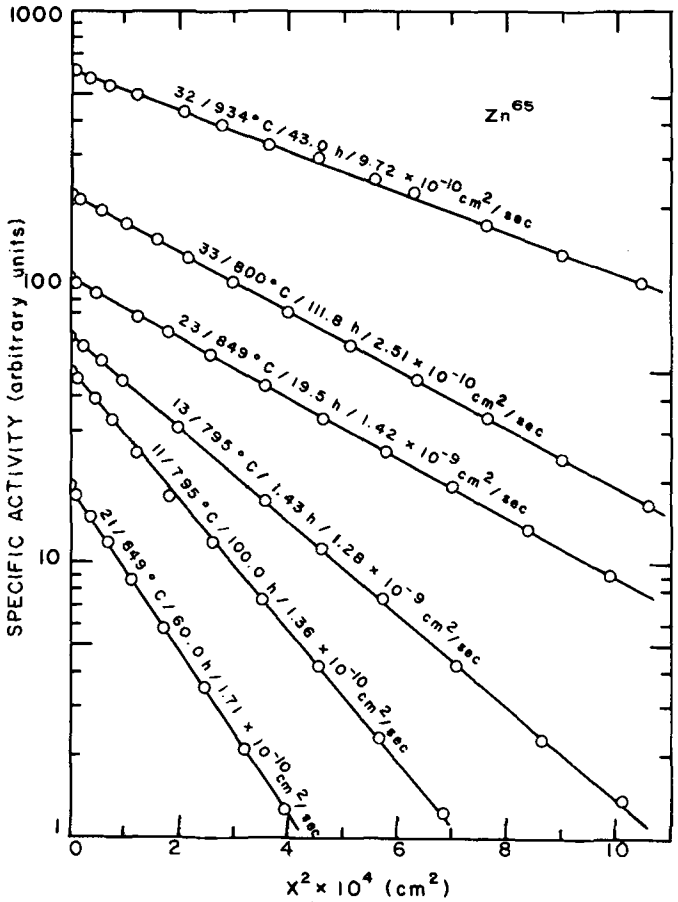

Fig. 2—Representative penetration plots for the diffusion of Zn^{65} in Cu-Ni-Zn alloys.

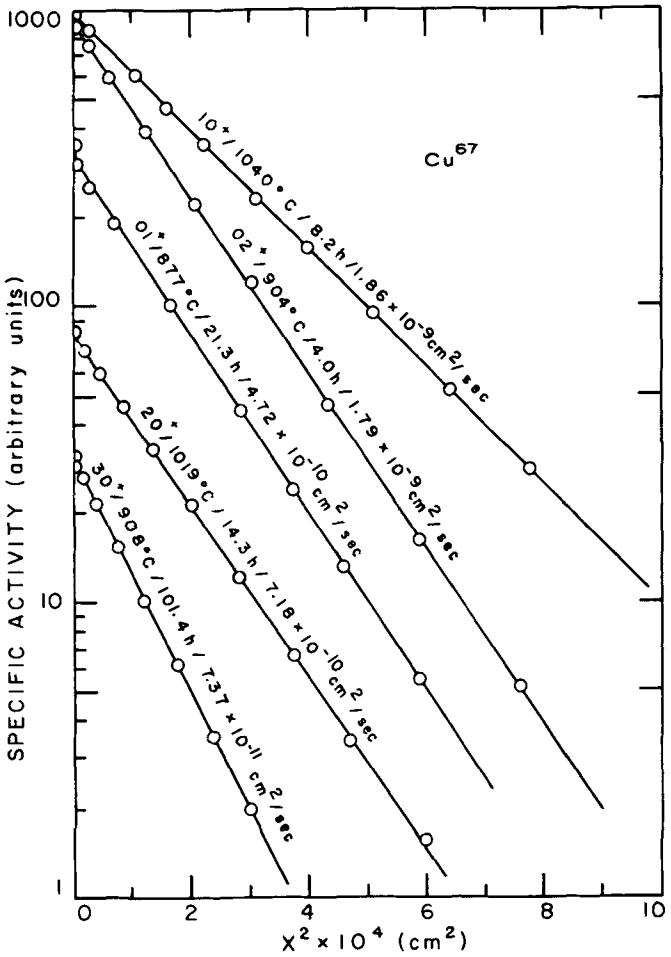

Fig. 3—Typical penetration plots for the diffusion of Cu^{67} in Cu-Ni and Cu-Zn alloys.

each of the tracers. These contours were determined graphically from the correlations resulting from the nonlinear least squares computer analysis of the data. The computation yielded the following empirical relationships for data obtained at 900°C:

$$\log_{10} D^*_{Zn} = -3.20N_{Ni} + 5.21N_{Zn}^{1.25} - 9.00$$
$$\log_{10} D^*_{Cu} = -3.53N_{Ni}^{1.16} + 3.60N_{Zn}^{1.02} - 9.46 \qquad [1]$$
$$\log_{10} D^*_{Ni} = -4.05N_{Ni}^{1.30} + 3.28N_{Zn}^{1.07} - 9.96$$

where N_{Ni} and N_{Zn} are the atom fractions of nickel and zinc, respectively. A visual assessment of the validity of this fit may be obtained from Figs. 10 and 11. The dependence of each of the tracer diffusivities upon zinc content in binary Cu-Zn alloys is shown in Fig. 10; the circles are measured diffusivities, and the curves shown are plotted from the computed least squares equation. Fig. 11 shows the concentration dependence of D^* in binary Cu-Ni alloys.

Figs. 12, 13, and 14 represent the concentration dependence of log D^* in ternary composition space. In each case, a three dimensional plot of the variation of diffusivity with composition is shown for a specific tracer.

These plots clearly show the general trend in composition dependence observed in all of the data obtained. Diffusivities are highest in binary, high zinc alloys, and lowest in binary, high nickel alloys. The range of diffusivities between these two extremes varies over about two orders of magnitude for each isotope. At any composition, the ratio of the three diffusivities is about the same, and is given by

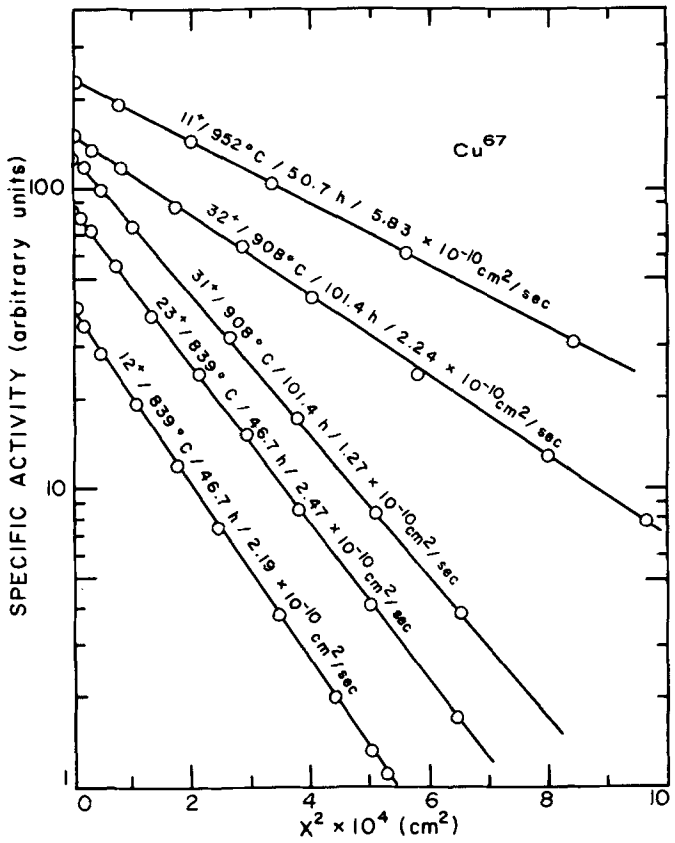

Fig. 4—Typical penetration plots for the diffusion of Cu^{67} in Cu-Ni-Zn alloys.

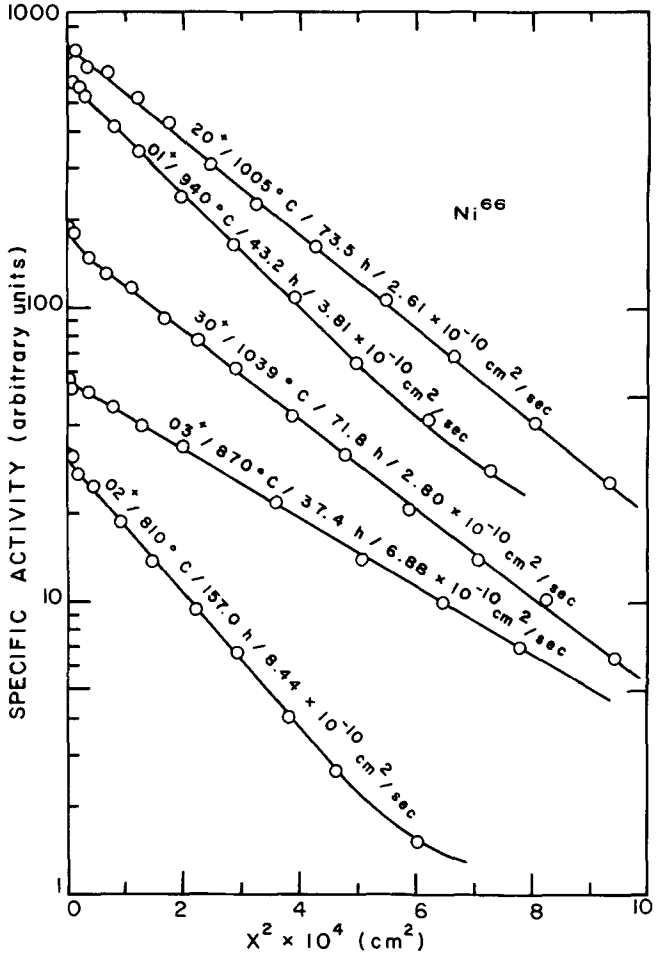

Fig. 5—Representative penetration plots for the diffusion of Ni^{66} in Cu-Ni and Cu-Zn alloys.

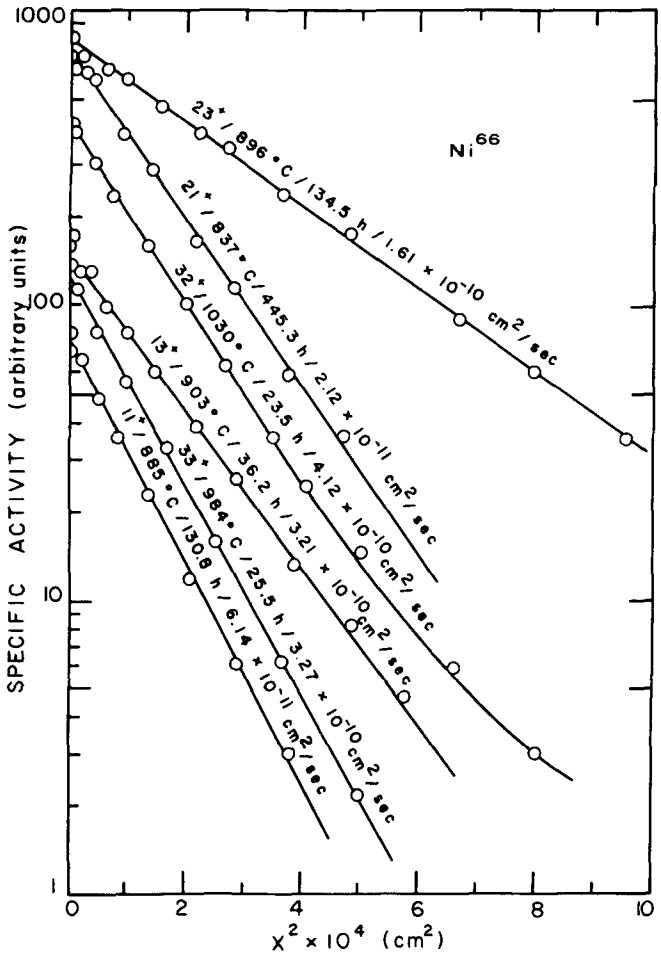

Fig. 6—Representative penetration plots for the diffusion of Ni^{66} in Cu-Ni-Zn alloys.

$D^*_{Zn}:D^*_{Cu}:D^*_{Ni}$ as 9:3:1. The surface of Zn^{65}, Fig. 12, is smooth over the whole composition region; the corresponding surfaces for Cu^{67}, Fig. 13, and Ni^{66}, Fig. 14, show some rumpling, with a relative minimum in the range of the 11 alloy.

Temperature Dependence and Activation Energies

Although no previous measurements of tracer diffusivities have been made in this ternary system, it is possible to compare some of the measured D^* values with independent work in the two binary systems involved. These comparisons are most readily made from Arrhenius plots of data from the present study displayed with observations of other investigators. Such a comparison is shown in Fig. 15 for all three tracers diffusing in pure copper. Similar comparisons may be made for zinc and copper tracers diffusing in brass alloys containing approximately 30 at. pct Zn, as shown in Fig. 16. Fig. 17 shows a similar comparison for Ni^{66} and Cu^{67} diffusing in nominally 20 at. pct Ni Cu-Ni alloys. In all cases data obtained in the present study fall within the range of values for comparable determinations by independent investigators. In some cases small differences observed may be rationalized on the basis of minor differences in composition in the alloys used in various studies.

The temperature dependence of diffusivities of each of the tracers in each of the sixteen compositions

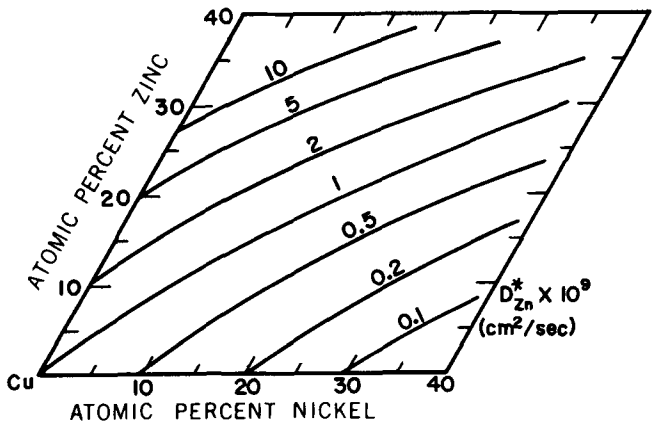

Fig. 7—Concentration dependence of D^*_{Zn} in copper-rich Cu-Ni-Zn alloys at 900°C.

studied are reported in Arrhenius plots in Figs. 18 to 29. Activation energies calculated from least-squares analyses of these plots are given in Tables VIII, IX, and X.

The composition dependence of the activation energies may be represented by

$$Q^*_{Zn}\ (\text{kcal/mol}) = 29.2N_{Ni}^{1.03} - 50.4N_{Zn}^{1.8} + 45.5$$

$$Q^*_{Cu}\ (\text{kcal/mol}) = 481.2(1 + 2.37N_{Ni}^{4.55}) \times (1 - 0.07N_{Zn}^{1.29}) - 432.3 \quad [2]$$

Table V. Tabulated Data for Tracer Diffusion of Zn^{65} in Alloys of the Cu-Ni-Zn System

Alloy Designation	Composition At. Pct Cu	Ni	Zn	Temp, °C	Time, hr	Diffusion Coefficient $D^*_{Zn} \times 10^{10}$, cm^2/sec
00	99.99	–	–	800	160.00	1.62
				807	105.50	1.64
				842	30.00	3.57
				846	64.83	3.86
				1009	9.90	48.0
				1040	36.53	75.1
01	89.9	–	10.1	748	96.00	1.18
				795	56.00	3.06
				849	48.40	8.50
				901	15.00	23.3
				979	24.50	65.5
02	79.5	–	20.5	748	77.00	3.10
				800	21.00	9.79
				850	6.00	22.0
				900	6.00	49.3
				940	5.00	85.2
03	69.8	–	30.2	700	150.00	4.67
				750	49.33	13.7
				798	21.00	33.2
				850	3.25	66.8
				868	24.00	102.0
				902	3.00	158.0
10	90.7	9.3	–	795	221.50	0.659
				849	90.12	2.15
				850	203.30	1.56
				897	63.10	3.85
				934	43.10	7.11
				960	51.70	11.8
				1032	4.90	40.5
				1040	36.53	43.4
11	80.4	9.3	10.3	750	109.65	0.486
				795	100.00	1.36
				849	55.25	3.88
				897	31.40	9.55
				1005	18.53	49.2
12	70.2	9.3	20.5	750	109.65	1.33
				795	32.50	3.40
				848	15.98	10.5
				940	10.67	47.0
				976	4.60	88.5
13	60.1	9.1	30.8	700	150.00	1.99
				748	75.40	4.71
				795	14.25	12.8
				852	17.50	47.8
				901	6.30	61.6
20	81.8	18.2	–	795	378.80	0.267
				853	289.16	1.09
				900	127.50	2.51
				934	20.00	4.71
				1005	11.50	14.8
21	70.8	18.8	10.4	800	165.00	0.699
				849	60.00	1.71
				900	48.00	5.34
				975	20.25	16.8
				1040	36.53	39.5
22	60.6	18.6	20.8	800	214.00	1.66
				849	76.95	4.36
				850	94.20	5.60
				902	25.50	12.8
				979	29.51	40.3
				1011	5.10	74.7

Table V. (Contd)

Alloy Designation	Composition At. Pct Cu	Ni	Zn	Temp, °C	Time, hr	Diffusion Coefficient $D^*_{Zn} \times 10^{10}$, cm^2/sec
23	50.3	18.7	31.0	748	77.00	1.98
				800	41.00	6.10
				849	19.50	14.2
				901	15.00	33.5
				940	7.25	68.1
30	71.4	28.6	–	870	301.00	0.751
				886	129.75	0.664
				900	313.00	1.24
				950	100.33	3.51
				1005	20.50	8.54
				1041	39.20	13.9
				1080	20.00	24.5
31	61.2	28.2	10.6	855	311.80	0.909
				900	127.50	2.30
				956	118.00	7.10
				995	75.75	13.2
				1041	39.20	24.8
32	50.8	28.2	21.0	800	189.00	0.795
				849	74.75	2.51
				850	203.30	2.33
				934	43.00	9.72
				1005	18.53	31.1
33	40.7	27.9	31.4	760	377.00	1.07
				800	111.83	2.51
				850	7.50	6.39
				899	24.00	15.1
				976	4.25	59.8

These empirical relations were obtained by a nonlinear least square computer analysis, and express Q^*_{Zn} and Q^*_{Cu} with an accuracy of 1 kcal/mol over the composition range studied. A similar relationship for Q^*_{Ni} could not be generated within acceptable error limits.

Three dimensional plots of the activation energy surface over the composition plane are presented in Fig. 30 (Zn^{65}), Fig. 31 (Cu^{67}), and Fig. 32(Ni^{66}). In order to show the composition variation in the best perspective, it is necessary to view each of these surfaces from a different direction; it is essential to have the relative orientation of the composition plane clearly in mind when comparing these figures.

Figs. 30 to 32 establish the following observations: 1) all activation energies fall approximately in the range from 40 to 55 kcal, for all three tracers, and over the entire composition range studied. 2) Activation energies for diffusion of all three tracers is highest for binary, high-nickel alloys, and decreases to lowest for binary, high-zinc alloys. 3) With very few exceptions, the activation energies are in the order $Q^*_{Ni} > Q^*_{Cu} > Q^*_{Zn}$. 4) Activation energies for copper and nickel show a trough at about 20 at. pct Ni; this trough is more evident for the nickel tracer, which indeed shows a pronounced minimum on the binary axis.

The frequency factor, D^*_0, was also calculated for each of the tracers at each composition from the intercepts of the corresponding Arrhenius plots. These results are summarized in Tables VIII, IX, and X, and presented graphically in Figs. 33, 34, and 35. The concentration dependences of the D^*_0 in ternary space displayed in these plots are qualitatively similar to those

Table VI. Tabulated Data for Tracer Diffusion of Cu^{67} in Alloys of the Cu-Ni-Zn System

Alloy Designation	Composition, At. Pct Cu	Ni	Zn	Temp, °C	Time, hr	Diffusion Coefficient $D^*_{Cu} \times 10^{10}$, cm^2/sec
00+	99.999	–	–	740	101.83	0.115
				807	95.33	0.501
				830	47.00	0.858
				912	38.42	3.55
				937	18.50	5.74
				975	14.59	11.0
				1010	13.83	17.5
				1045	18.58	30.2
01+	90.25	–	9.75	786	94.33	0.746
				807	35.33	1.21
				830	47.00	1.89
				870	21.28	4.14
				877	21.33	4.72
				904	15.33	7.20
				912	38.47	7.85
				937	18.50	12.6
				975	14.59	25.5
				1010	13.83	39.5
02+	80.08	–	19.92	745	27.33	0.904
				786	58.42	2.14
				807	35.33	3.23
				877	10.67	11.7
				904	4.00	17.9
				912	38.42	22.3
				937	18.50	34.0
03+	70.94	–	29.06	720	27.33	1.97
				750	38.00	3.78
				780	35.50	6.30
				807	12.42	10.2
				839	12.00	17.3
				869	6.00	28.4
				876	8.85	33.8
				904	4.00	49.3
10+	90.08	9.92	–	904	44.75	2.02
				946	27.75	3.97
				965	10.33	5.37
				1003	12.00	10.3
				1019	12.42	13.2
				1040	8.17	18.6
				1050	6.00	20.1
11+	82.72	12.55	4.73	785	143.00	0.254
				808	155.67	0.397
				838	72.25	0.758
				866	75.75	1.21
				904	22.25	2.50
				952	50.67	5.83
				973	11.67	8.40
				1003	12.00	13.9
12+	72.04	11.21	16.75	740	101.83	0.280
				808	72.58	1.16
				839	46.67	2.19
				866	75.75	3.50
				877	16.33	4.13
				877	21.33	4.14
				904	15.33	7.03
				973	11.67	21.1
				1003	12.00	33.7
13+	65.06	10.82	24.12	783	35.50	1.70
				807	47.50	2.48
				809	23.17	2.74
				839	12.00	4.39
				868	9.00	7.81
				904	23.58	14.0
				937	20.25	23.0
				943	14.17	26.6

Table VI. (Contd)

Alloy Designation	Composition, At. Pct Cu	Ni	Zn	Temp, °C	Time, hr	Diffusion Coefficient $D^*_{Cu} \times 10^{10}$, cm^2/sec
20+	80.28	19.72	–	832	163.17	0.316
				904	68.42	1.14
				908	101.42	1.21
				937	27.25	2.31
				968	35.10	3.61
				1019	14.33	7.18
				1065	10.16	14.2
				1088	7.00	22.1
21+	69.68	19.42	10.90	800	176.33	0.318
				838	155.33	0.725
				866	75.75	1.14
				904	44.75	2.10
				952	50.67	4.84
				1003	12.00	11.7
				1050	6.00	22.8
22+	63.95	20.80	15.25	752	101.83	0.207
				800	167.33	0.535
				808	155.67	0.667
				838	72.25	1.08
				904	22.25	3.54
				942	27.75	6.45
				949	11.67	7.31
				973	11.67	10.2
				1003	12.00	17.4
23+	55.17	50.59	24.24	748	100.00	0.447
				786	94.33	0.953
				807	95.33	1.43
				839	46.67	2.47
				866	75.75	3.97
				912	38.42	8.56
				937	18.50	13.7
				949	14.17	15.1
30+	71.73	28.27	–	908	101.42	0.737
				938	89.58	1.19
				952	71.50	1.80
				970	61.90	2.18
				1010	22.83	4.40
				1017	27.00	5.02
				1040	19.00	6.56
				1065	10.16	9.72
				1088	7.00	14.4
				11113	6.33	19.7
31+	60.97	29.49	9.54	904	68.42	1.03
				908	101.42	1.27
				952	71.50	2.84
				968	35.10	3.43
				1003	12.00	6.01
				1019	14.33	8.27
				1050	6.00	13.4
				1072	11.25	17.7
32+	47.12	33.08	19.80	866	75.75	1.02
				902	34.25	1.84
				908	101.42	2.24
				942	13.50	4.13
				952	20.33	5.42
				970	11.75	7.37
				1003	12.00	12.5
				1065	10.16	25.5
33+	40.30	30.70	29.00	807	95.33	0.498
				808	72.58	0.474
				839	46.67	0.913
				857	30.25	1.28
				870	21.38	1.66
				904	23.58	3.22
				937	18.50	6.65
				952	20.33	6.83
				966	11.75	9.75

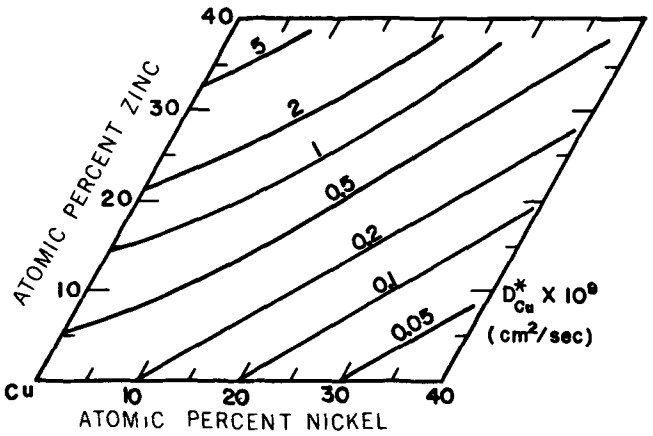

Fig. 8—Concentration dependence of D^*_{Cu} in copper-rich Cu-Ni-Zn alloys at 900°C.

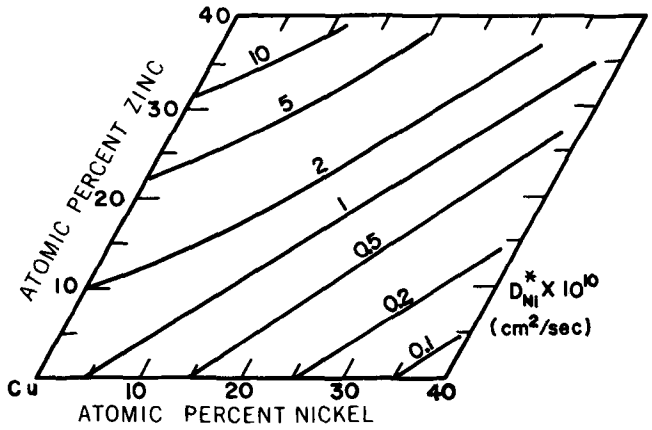

Fig. 9—Concentration dependence of D^*_{Ni} in copper-rich Cu-Ni-Zn alloys at 900°C.

observed for the activation energies. An important exception to this agreement is observed in the copper corner of the plot for Zn^{65}, where D^*_0 has anomalously low values.

DISCUSSION

The experimental observations reported in the previous section may be divided into two categories: 1) the variation of the diffusivities with composition, and 2) the variation of the activation energies and frequency factors with composition. In this section an attempt is made to show that the behavior observed in these two groupings is consistent with mechanical (size), electronic (effective electron concentration), and thermodynamic effects in Cu-Ni-Zn alloys.

Properties of Cu-Ni-Zn Alloys

MECHANICAL EFFECTS

An estimate of the relative sizes of the three species in solid solution may be obtained from lattice parameter measurements, and from an analysis of the density measurements presented in Table II. When these latter are converted to molar volumes and plotted vs composition, Fig. 36, it is found that the resulting surface may be described by the equation:

$$V = 7.09N_{Cu} + 6.60N_{Ni} + 8.47N_{Zn} \quad [3]$$

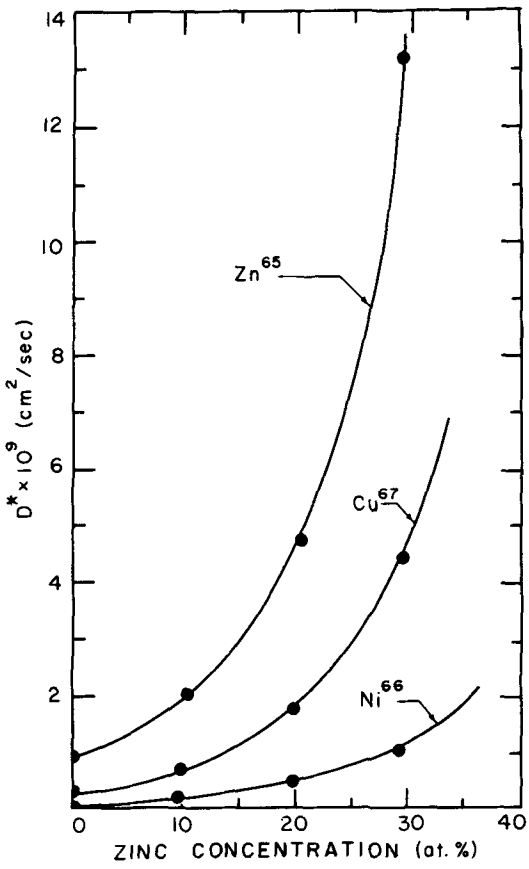

Fig. 10—Concentration dependence of D^*_{Zn}, D^*_{Cu}, and D^*_{Ni} at 900°C in the Cu-Zn system over the range 0 to 30 at. pct Zn.

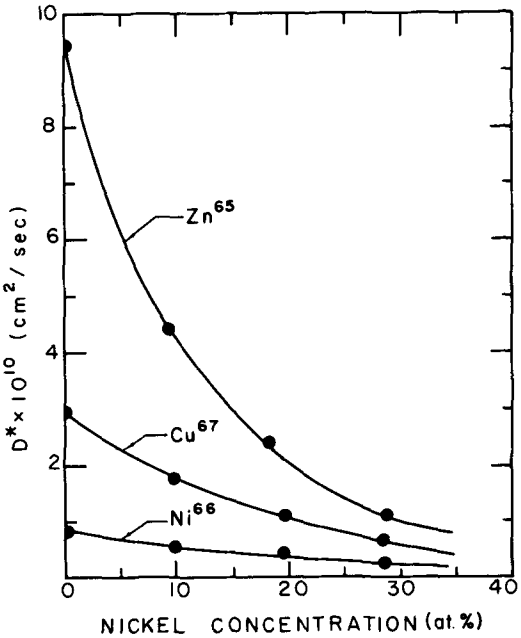

Fig. 11—Concentration dependence of D^*_{Zn}, D^*_{Cu}, and D^*_{Ni} at 900°C in the Cu-Ni system over the range 0 to 30 at. pct Zn.

with an error of less than 1.5 pct. Clearly, the molar volume increases as zinc is added, and decreases as nickel is added to any alloy. Eq. [3] can be expressed in terms of the partial molar volumes V_i of the three components, since[16]

$$V = \overline{V}_{Cu}N_{Cu} + \overline{V}_{Ni}N_{Ni} + \overline{V}_{Zn}N_{Zn} \quad [4]$$

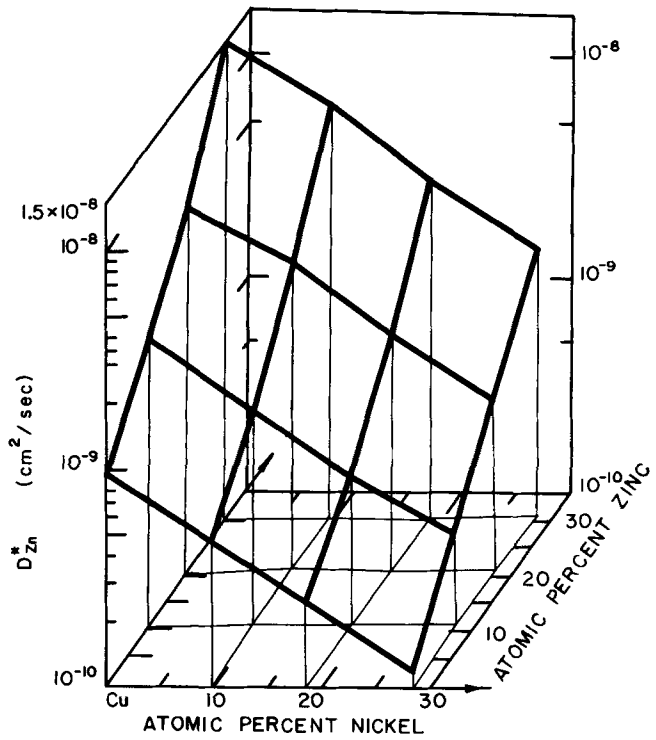

Fig. 12—Log D^*_{Zn} vs concentration at 900°C.

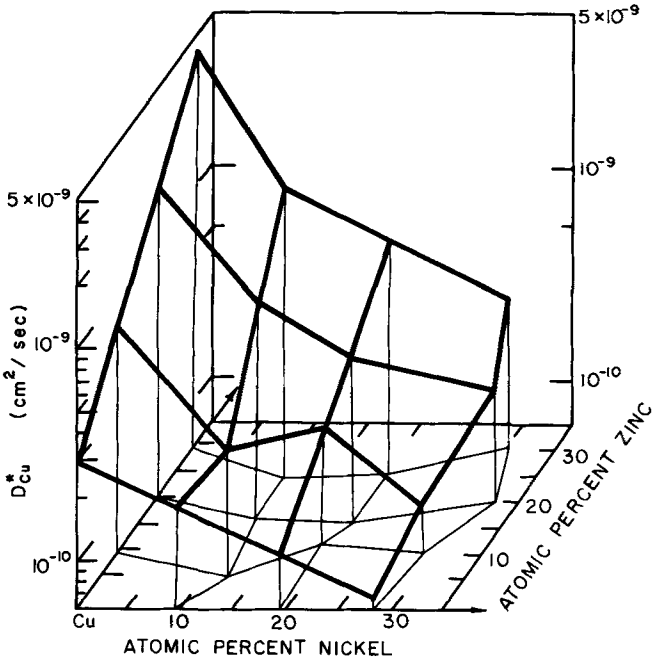

Fig. 13—Log D^*_{Cu} vs concentration at 900°C.

Comparison with Eq. [3] shows that the partial molar volumes are constant over the composition range, and have the values:

$$\overline{V}_{Cu} = 7.09 \text{ cu cm/mol}$$
$$\overline{V}_{Ni} = 6.60 \text{ cu cm/mol} \quad [5]$$
$$\overline{V}_{Zn} = 8.47 \text{ cu cm/mol}$$

The molar volumes of pure copper, nickel, and zinc are respectively 7.09, 6.59, and 9.17 cu cm/mol. Thus, this system behaves nearly ideally with respect to the volume changes on mixing for copper and nickel, but not with respect to zinc.

Room temperature measurements of the lattice parameter of alloys in this composition range can be represented by the equation:[17]

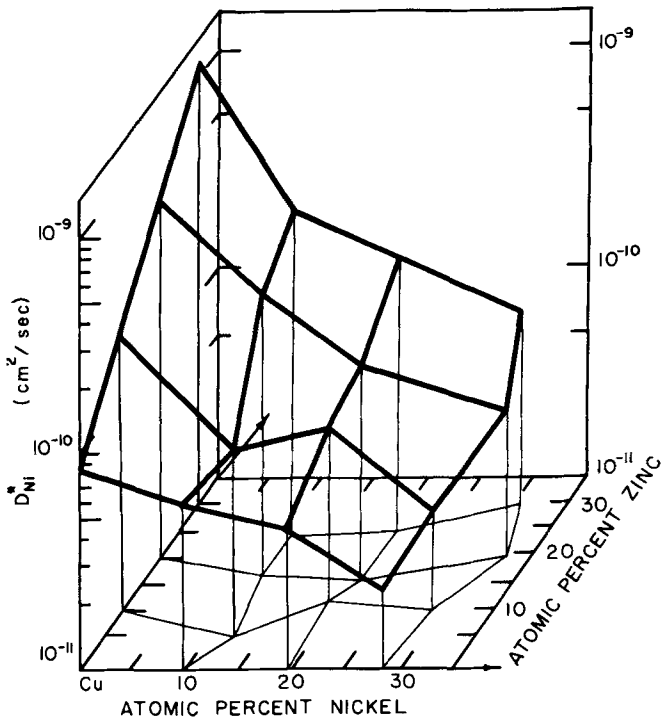

Fig. 14—Log D^*_{Ni} vs concentration at 900°C.

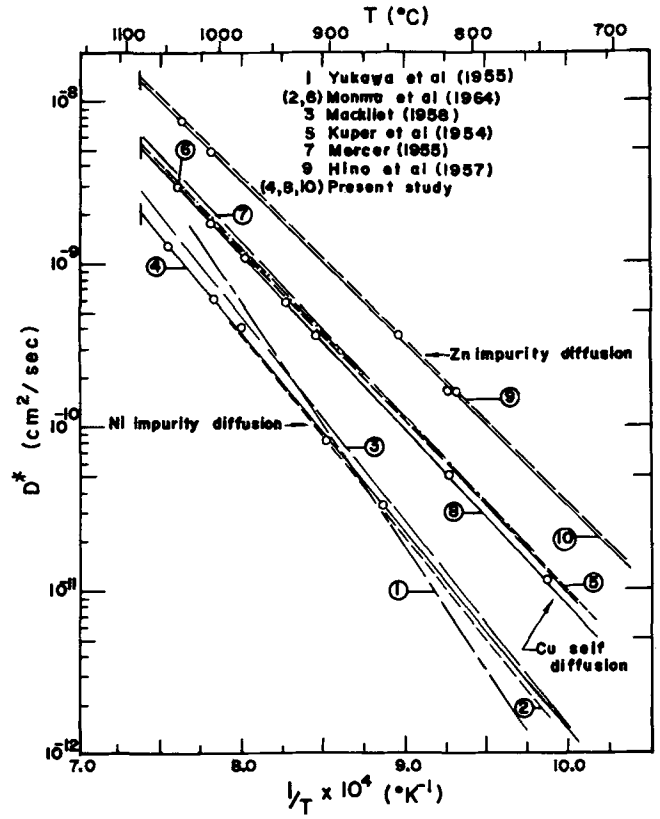

Fig. 15—Comparison of the temperature dependence of D^*_{Zn}, D^*_{Cu}, and D^*_{Ni} in pure copper obtained in the present study and earlier work.

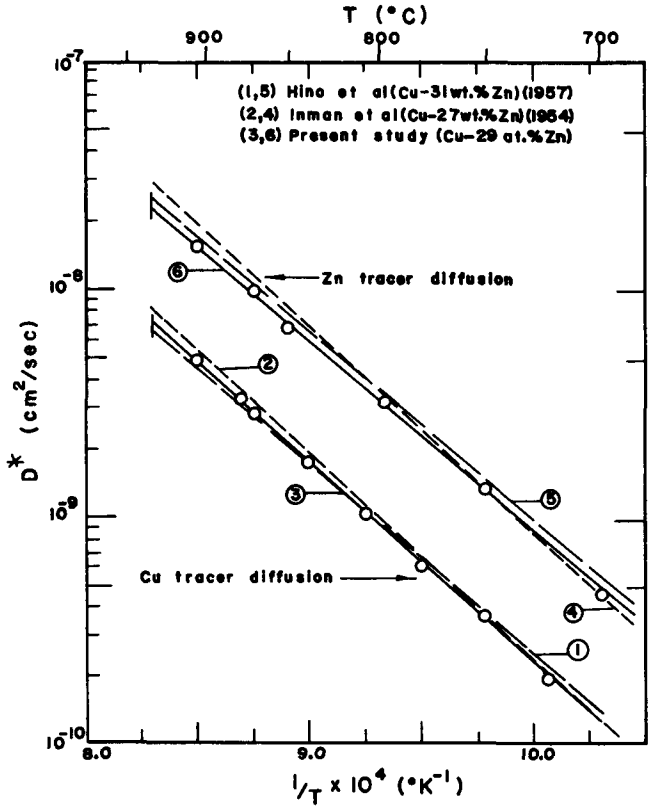

Fig. 16—Comparison of the temperature dependence of D^*_{Cu} and D^*_{Zn} in Cu-Zn alloys obtained in the present study and earlier work.

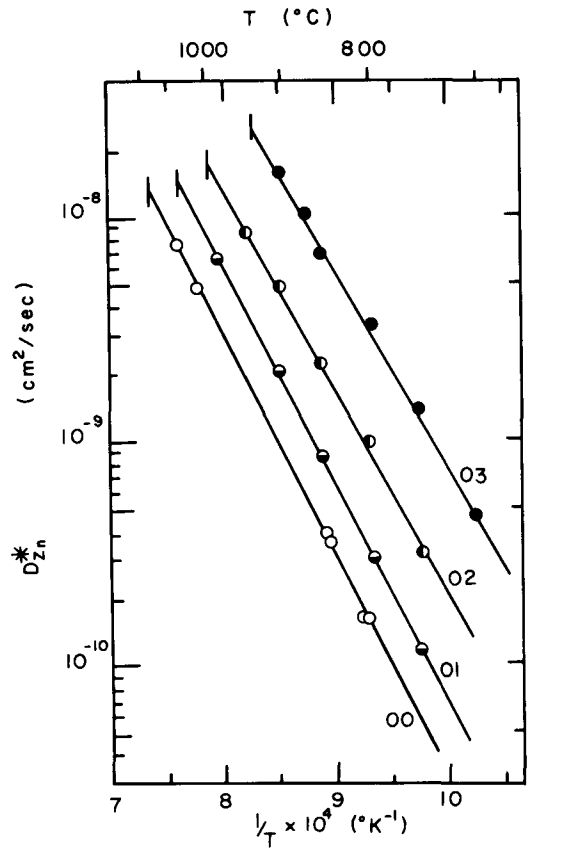

Fig. 18—Temperature dependence of D^*_{Zn} in Cu-Zn alloys and pure copper.

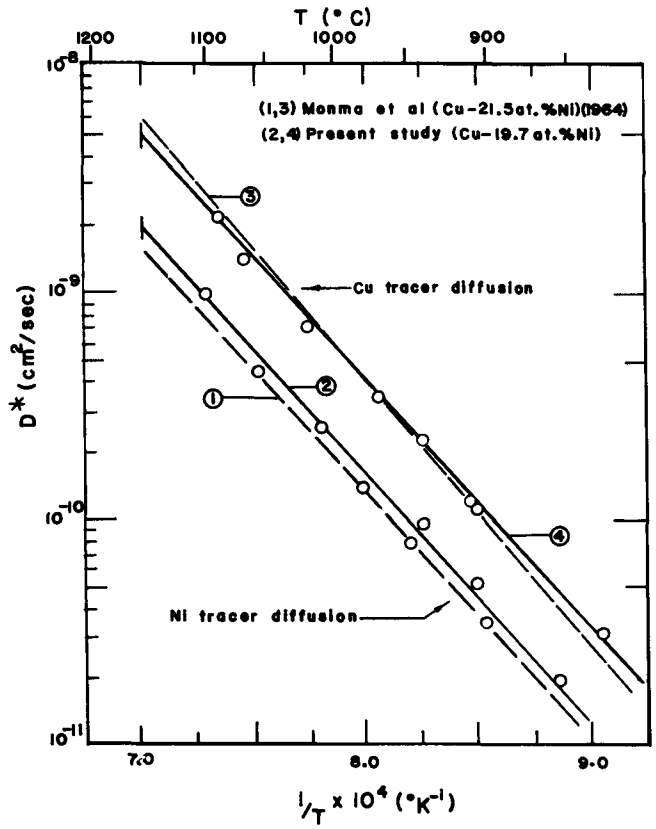

Fig. 17—Comparison of the temperature dependence of D^*_{Cu} and D^*_{Ni} in Cu-Ni alloys obtained in the present study and earlier work.

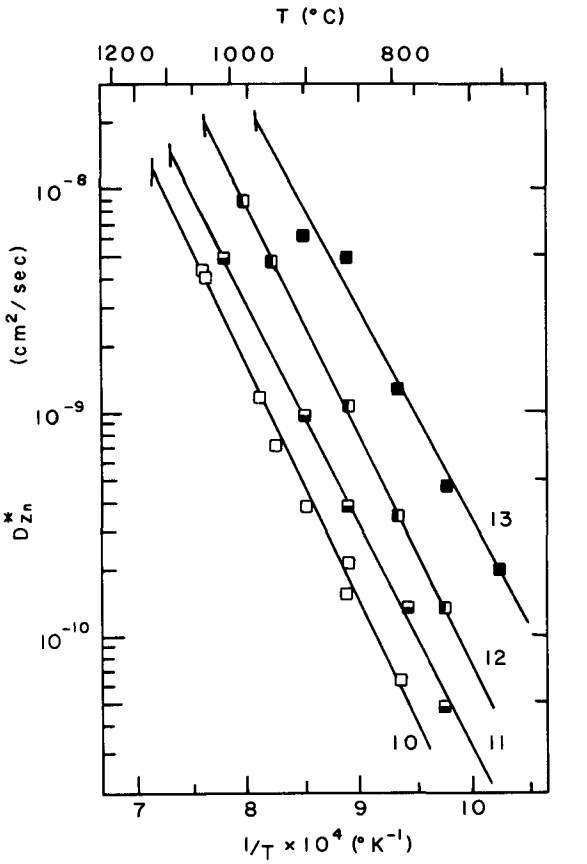

Fig. 19—Temperature dependence of D^*_{Zn} in Cu-Ni-Zn alloys containing approximately 9 at. pct Ni.

Table VII. Tabulated Data for Tracer Diffusion of Ni^{66} in Alloys of the Cu-Ni-Zn System

Alloy Designation	Composition, At. Pct Cu	Ni	Zn	Temp, °C	Time, hr	Diffusion Coefficient $D^*_{Ni} \times 10^{10}$, cm^2/sec
00+	99.999	–	–	855	172.45	0.331
				903	108.38	0.821
				980	76.42	4.09
				1005	34.60	6.04
				1055	70.50	13.0
01+	90.25	–	9.75	791	346.25	0.200
				845	106.00	0.606
				872	200.00	1.02
				880	332.34	1.31
				900	51.32	1.86
				929	110.00	3.10
				940	43.17	3.81
				970	50.00	6.13
				974	76.17	7.56
				981	29.33	7.87
				982	39.50	8.53
				983	71.75	8.56
				995	51.17	10.5
02+	80.08	–	19.92	777	234.50	0.440
				784	236.00	0.461
				810	157.00	0.844
				837	155.70	1.39
				871	85.00	2.75
				872	72.00	2.85
				880	89.00	3.37
				890	56.00	3.80
				906	47.00	4.60
				946	23.00	9.13
03+	70.94	–	29.06	739	143.50	0.542
				755	178.50	0.802
				779	99.50	1.37
				784	236.00	1.45
				794	274.75	1.70
				824	23.00	2.95
				843	23.00	4.01
				870	37.40	6.88
				874	27.50	7.15
				895	51.30	9.88
10+	90.08	9.92	–	929	140.50	1.02
				937	317.15	1.20
				950	164.00	1.58
				970	136.00	2.14
				973	106.33	2.19
				983	71.75	2.32
				997	139.75	3.11
				1020	72.00	4.58
				1027	24.00	5.01
				1074	44.00	11.5
				1106	70.80	17.0
11+	82.72	12.55	4.73	779	307.00	0.064
				880	153.67	0.476
				885	130.80	0.614
				894	154.67	0.677
				901	106.00	0.792
				929	140.50	1.18
				949	87.33	1.77
				970	50.00	2.29
				974	76.77	2.51
				983	71.75	3.19
				984	25.00	2.91
				996	51.17	3.72
				1020	72.00	5.11
				1027	24.00	6.62
12+	72.04	11.21	16.75	784	236.00	0.232
				811	326.00	0.413
				834	240.50	0.530
				837	206.30	0.579

Table VII. (Contd)

Alloy Designation	Composition, At. Pct Cu	Ni	Zn	Temp, °C	Time, hr	Diffusion Coefficient $D^*_{Ni} \times 10^{10}$, cm^2/sec
				870	222.16	1.23
				901	106.00	2.02
				906	113.60	2.37
				929	110.00	3.31
				946	71.40	4.48
				974	76.17	7.21
				981	44.50	7.53
				984	25.50	7.84
				999	4.25	10.4
13+	65.06	10.82	24.12	794	274.75	0.493
				825	119.58	0.798
				855	48.25	1.49
				870	332.34	2.04
				872	200.00	1.99
				875	46.67	2.20
				903	36.20	3.21
				934	58.42	5.47
				940	56.75	6.34
				946	37.40	6.57
				959	25.30	8.41
20+	80.28	19.72	–	855	261.70	0.196
				899	207.00	0.354
				904	220.80	0.534
				937	317.75	0.947
				946	155.90	0.796
				980	76.42	1.41
				1005	73.51	2.61
				1055	70.50	4.52
				1097	23.50	10.1
21+	69.68	19.42	10.90	837	445.30	0.212
				872	359.60	0.391
				906	149.00	0.759
				946	155.90	1.52
				981	44.50	2.64
				1041	28.30	6.92
22+	63.95	20.80	15.25	837	359.50	0.311
				874	141.50	0.586
				896	134.50	0.887
				929	140.50	1.50
				940	114.51	2.15
				982	77.83	3.48
				999	46.58	4.87
				1013	34.00	6.22
23+	55.17	20.59	24.24	791	346.25	0.197
				811	326.00	0.380
				837	206.30	0.598
				855	135.83	0.798
				874	414.10	1.02
				896	134.50	1.61
				901	106.00	1.89
				929	52.00	2.96
				934	58.42	3.01
				951	34.58	3.96
				983	71.75	6.70
30+	71.73	28.27	–	901	105.75	0.287
				904	547.00	0.245
				936	391.00	0.467
				946	468.50	0.542
				973	106.33	0.933
				981	236.00	1.09
				997	139.75	1.21
				1020	119.00	2.12
				1039	71.80	2.80
				1050	62.50	3.32
				1074	44.00	4.62
				1097	23.50	7.17
				1118	9.25	8.71
				1134	3.75	10.1

Table VII. (Contd)

Alloy Designation	Composition, At. Pct Cu	Ni	Zn	Temp, °C	Time, hr	Diffusion Coefficient $D^*_{Ni} \times 10^{10}$, cm²/sec
31+	60.97	29.49	9.54	904	452.20	0.335
				946	237.70	0.728
				973	106.33	1.18
				982	292.00	1.50
				1020	119.00	2.62
				1043	62.50	3.73
				1060	48.00	5.49
				1074	44.00	6.06
32+	47.12	33.08	19.80	870	332.30	0.265
				896	134.50	0.430
				929	14.50	0.840
				940	114.70	0.973
				973	106.30	1.78
				982	77.80	2.32
				999	46.60	2.85
				1030	23.50	4.12
				1041	28.30	5.43
				1050	62.50	6.41
33+	40.30	30.70	29.00	885	130.80	0.542
				901	106.00	0.775
				929	140.50	1.28
				949	87.33	1.70
				970	50.00	2.40
				974	76.17	2.80
				984	25.50	3.27
				995	59.17	3.97

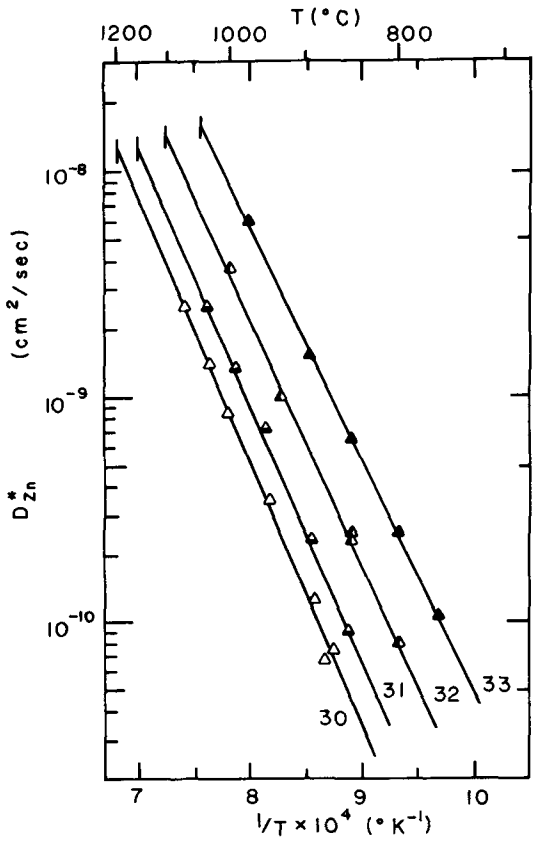

Fig. 21—Temperature dependence of D^*_{Zn} in Cu-Ni-Zn alloys containing approximately 28 at. pct Ni.

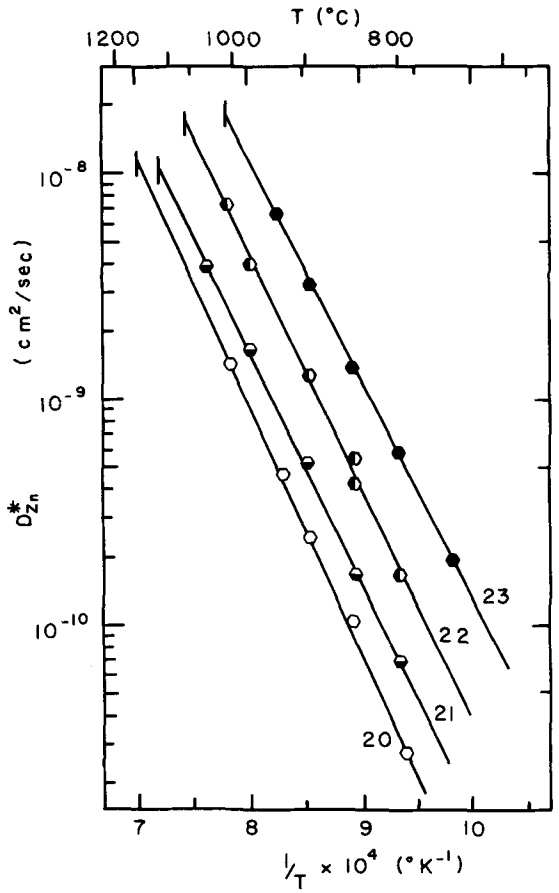

Fig. 20—Temperature dependence of D^*_{Zn} in Cu-Ni-Zn alloys containing approximately 19 at. pct Ni.

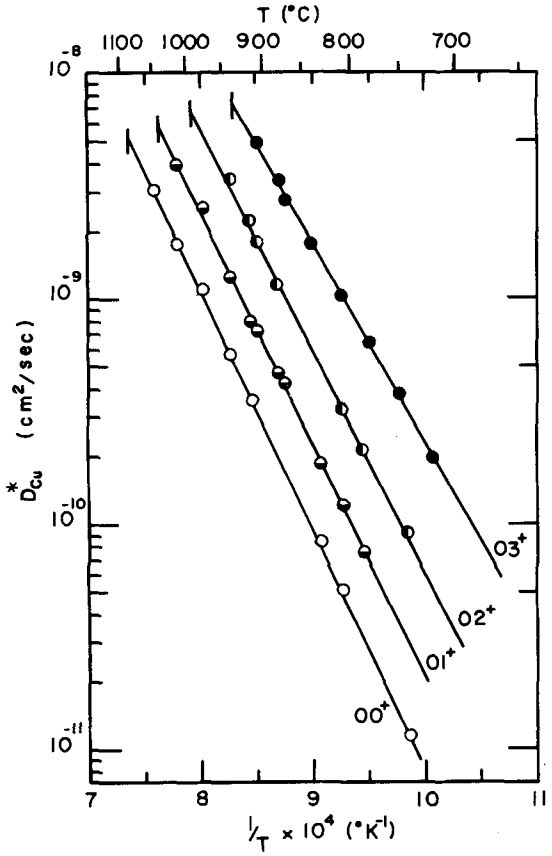

Fig. 22—Temperature dependence of D^*_{Cu} in Cu-Zn alloys and pure copper.

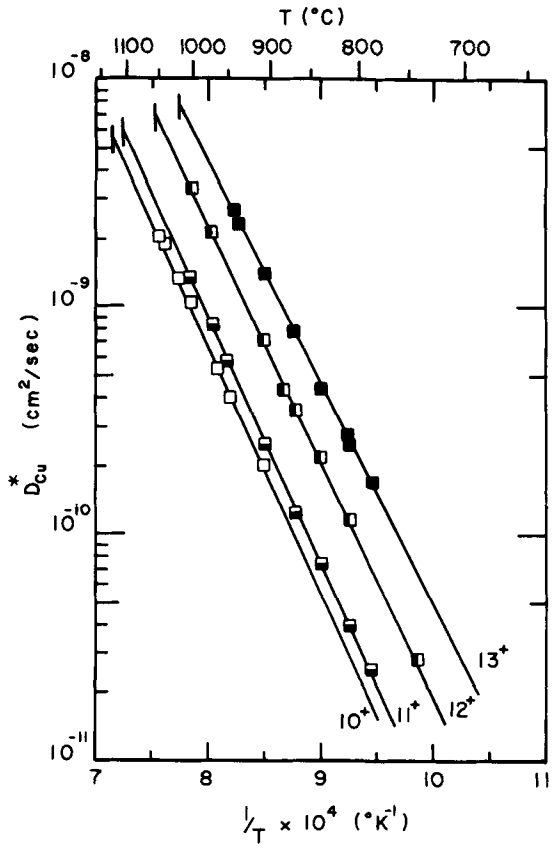

Fig. 23—Temperature dependence of D^*_{Cu} in Cu-Ni-Zn alloys containing approximately 11 at. pct Ni.

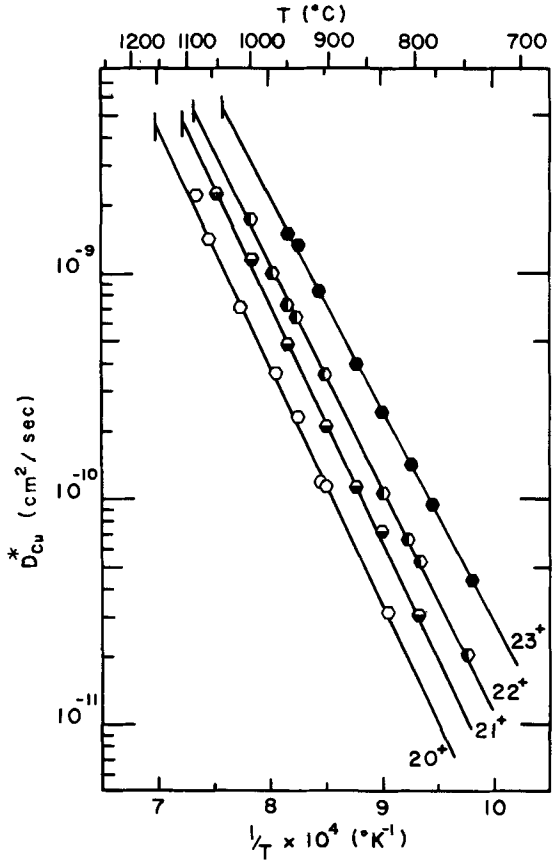

Fig. 24—Temperature dependence of D^*_{Cu} in Cu-Ni-Zn alloys containing approximately 20 at. pct Ni.

$$a_0 = 3.608N_{Cu} + 3.496N_{Ni} + 3.813N_{Zn} \quad [6]$$

This corresponds to effective atomic diameters in the ratio of 3.813:3.608:3.496, or 1.057:1.000:0.969. The cube root of the partial molar volumes in Eq. [5] are

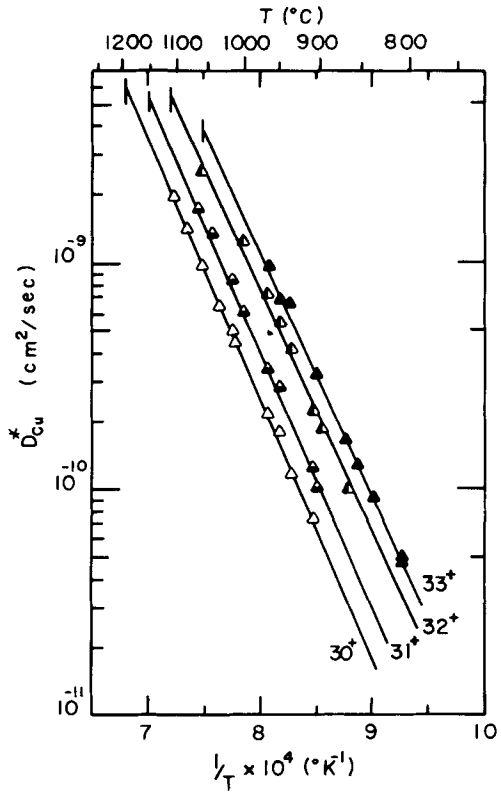

Fig. 25—Temperature dependence of D^*_{Cu} in Cu-Ni-Zn alloys containing approximately 30 at. pct Ni.

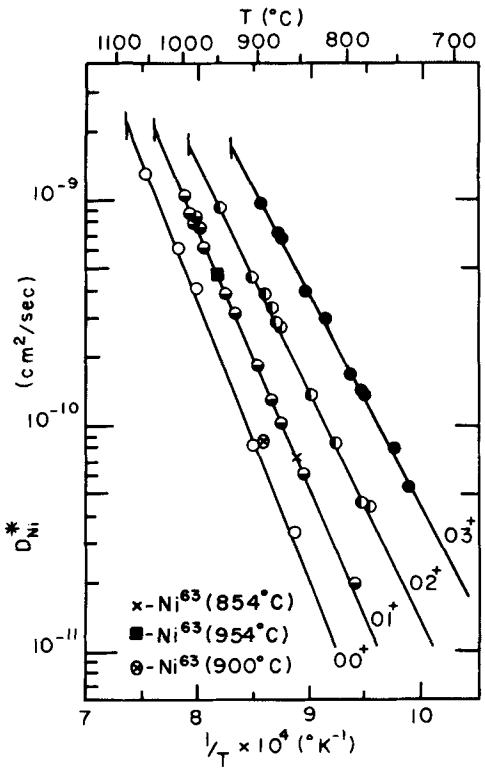

Fig. 26—Temperature dependence of D^*_{Ni} in Cu-Zn alloys and pure copper.

in the ratio 1.058:1.000:0.975. Thus, there is good agreement between lattice parameter and density measurements in this system.

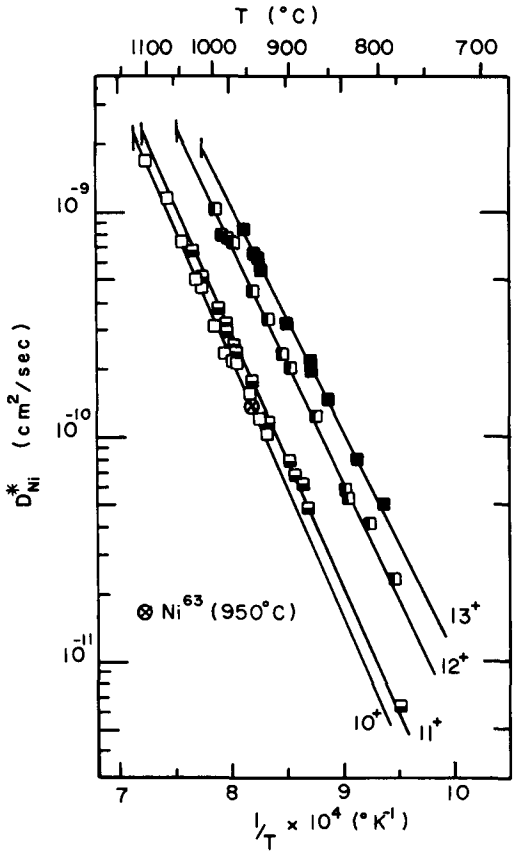

Fig. 27—Temperature dependence of D^*_{Ni} in Cu-Ni-Zn alloys containing approximately 11 at. pct Ni.

On the basis of these observations, it is concluded that the relative sizes of the three species are, in decreasing order: Zn, Cu, Ni. The absolute magnitudes of the atomic sizes, expressed as a volume or diameter, may be usefully regarded as independent of composition.

ELECTRONIC EFFECTS

On the basis of the location and shape of the $\alpha/(\alpha + \beta)$ phase boundary in this system, Hume-Rothery and Howarth[18] have suggested that the contribution of each of the three elements to the electron-to-atom ratio in these alloys should be: Cu—1 electron; Zn—2 electrons; Ni—0.6 electrons. Thus,

$$\frac{e}{a} = N_{Cu} + 0.6N_{Ni} + 2N_{Zn} \qquad [7]$$

Argent[19] has shown that this assumption leads to good fit in an empirical correlation between the thermodynamic properties of the alloys with size and electronic effects. These assumed electron concentrations are supported by similar correlations for other ternary systems. Hall effect measurements[20] also may be rationalized on the basis that the free electron concentration increases when zinc is added, and decreases as nickel is added to pure copper. Fig. 37 is a plot of the calculated electron-atom ratios as a function of composition. It is interesting that lines of constant electron concentration closely parallel lines of constant molar volume.

ORDERING AND CLUSTERING IN Cu-Ni-Zn ALLOYS

Direct X-ray measurements of the degree of ordering or clustering in this system are not practical, because

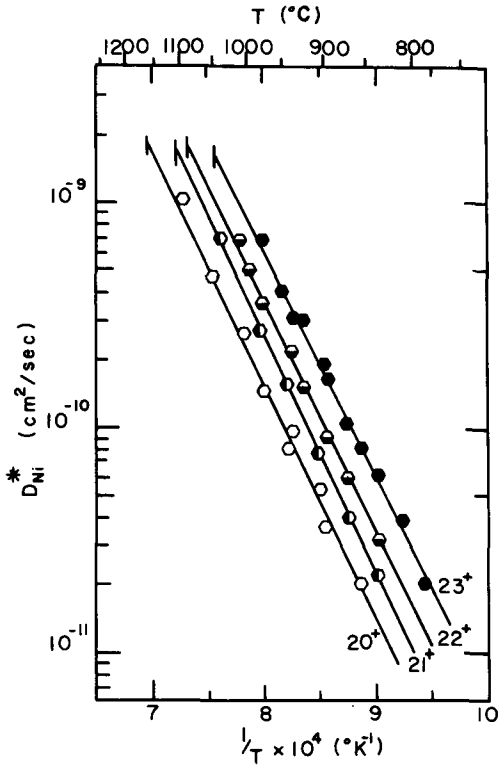

Fig. 28—Temperature dependence of D^*_{Ni} in Cu-Ni-Zn alloys containing approximately 20 at. pct Ni.

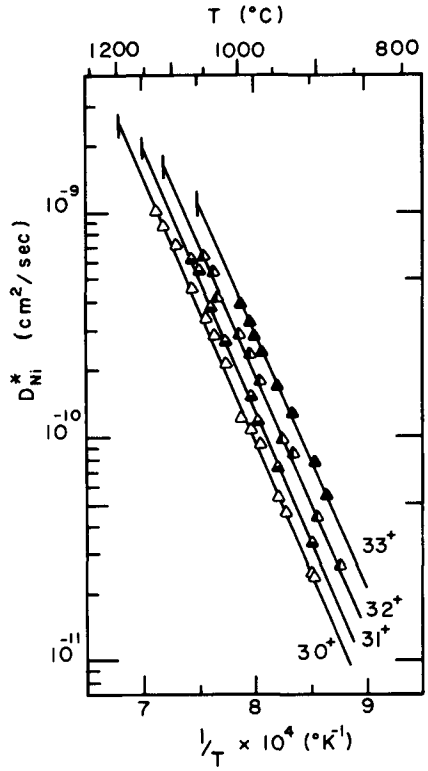

Fig. 29—Temperature dependence of D^*_{Ni} in Cu-Ni-Zn alloys containing approximately 30 at. pct Ni.

Table VIII. Diffusion Constants for Tracer Diffusion of Zn^{65} in Cu-Ni-Zn Alloys

Alloy Designation	Composition, At. Pct Cu	Ni	Zn	Experimental Temperature Range, °C	Diffusion Constants[a] D^*_{0Zn}, cm^2/sec	Q^*_{Zn}, kcal/mole
00	99.99	–	–	800-1040	$0.24^{+0.05}_{-0.05}$	45.1 ± 0.5
01	89.9	–	10.1	748-979	$0.64^{+0.07}_{-0.07}$	45.6 ± 0.2
02	79.5	–	20.5	748-940	$0.35^{+0.12}_{-0.09}$	42.2 ± 0.7
03	69.8	–	30.2	700-902	$0.32^{+0.10}_{-0.08}$	39.3 ± 0.6
10	90.7	9.3	–	795-1040	$0.36^{+0.22}_{-0.14}$	47.8 ± 1.1
11	80.4	9.3	10.3	750-1005	$0.49^{+0.05}_{-0.05}$	46.8 ± 0.2
12	70.2	9.3	20.5	750-976	$1.41^{+0.24}_{-0.23}$	46.9 ± 0.4
13	60.1	9.1	30.8	700-901	$0.39^{+0.62}_{-0.24}$	41.4 ± 3.2
20	81.8	18.2	–	795-1005	$0.89^{+0.36}_{-0.26}$	51.3 ± 0.8
21	70.8	18.8	10.4	800-1040	$0.36^{+0.17}_{-0.11}$	47.7 ± 0.9
22	60.6	18.6	20.8	800-1011	$1.09^{+0.60}_{-0.39}$	48.1 ± 1.0
23	50.3	18.7	31.0	748-940	$0.73^{+0.19}_{-0.15}$	44.7 ± 0.5
30	71.4	28.6	–	870-1080	$1.37^{+1.18}_{-0.63}$	54.1 ± 1.5
31	61.2	28.2	10.6	855-1041	$1.44^{+0.58}_{-0.41}$	52.6 ± 0.8
32	50.8	28.2	21.0	800-1005	$1.17^{+0.69}_{-0.40}$	49.9 ± 1.1
33	40.7	27.9	31.4	760-976	$1.13^{+0.39}_{-0.26}$	47.4 ± 0.7

[a]Error limits refer to the probable error.

Table IX. Diffusion Constants for Tracer Diffusion of Cu^{67} in Cu-Ni-Zn Alloys

Alloy Designation	Composition, At. Pct Cu	Ni	Zn	Experimental Temperature Range, °C	Diffusion Constants[a] D^*_{0Cu}, cm^2/sec	Q^*_{Cu}, kcal/mole
00+	99.999	–	–	740-1045	$0.30^{+0.04}_{-0.02}$	48.3 ± 0.2
01+	90.25	–	9.75	786-1010	$0.55^{+0.09}_{-0.08}$	47.8 ± 0.4
02+	80.08	–	19.92	745-937	$0.63^{+0.10}_{-0.09}$	45.9 ± 0.3
03+	70.94	–	29.06	720-904	$0.16^{+0.03}_{-0.02}$	40.5 ± 0.5
10+	90.08	9.92	–	904-1050	$0.37^{+0.09}_{-0.07}$	50.0 ± 0.5
11+	82.72	12.55	4.73	785-1003	$0.36^{+0.05}_{-0.05}$	49.2 ± 0.3
12+	72.04	11.21	16.75	740-1003	$0.33^{+0.04}_{-0.03}$	46.8 ± 0.2
13+	65.06	10.82	24.12	783-943	$0.21^{+0.04}_{-0.03}$	44.0 ± 0.4
20+	80.28	19.72	–	832-1088	$0.15^{+0.04}_{-0.03}$	49.0 ± 0.6
21+	69.68	19.42	10.90	800-1050	$0.18^{+0.05}_{-0.03}$	47.9 ± 0.5
22+	63.95	20.80	15.25	752-1003	$0.10^{+0.01}_{-0.01}$	45.4 ± 0.3
23+	55.17	20.59	24.24	748-949	$0.11^{+0.01}_{-0.02}$	43.9 ± 0.3
30+	71.73	28.27	–	908-1113	$0.34^{+0.08}_{-0.06}$	52.2 ± 0.5
31+	60.97	29.49	9.54	904-1050	$0.55^{+0.17}_{-0.13}$	52.2 ± 0.7
32+	47.12	33.08	19.80	866-1065	$0.58^{+0.33}_{-0.21}$	50.8 ± 1.1
33+	40.30	30.70	29.00	807-966	$0.72^{+0.25}_{-0.19}$	50.3 ± 0.7

[a]Error limits refer to the probable error.

the three elements are adjacent in the periodic table, and have similar scattering factors. Indirect evidence is available from activity data, Hall effect and electrical resistivity measurements, and observations of the specific heat of alloys in this system.

Measurements of the activity of zinc as a function of composition in this system[19] show a significant negative departure from ideality for that component over the whole composition range of interest in the present diffusion study. In the zeroth order quasichemical description of solutions, this implies a tendency toward ordering of zinc in the system. On the other hand, binary Cu-Ni alloys show a strong positive departure from ideality.[20] According to the quasichemical theory, in simple systems this implies a tendency toward clustering. At the high-copper end of the binary composition range clustering of nickel atoms would be expected. These implications are not always fulfilled, even in binary systems. Argent points out that the lines of constant activity coefficient for zinc in the composition plane in this system are closely parallel to lines of constant electron-to-atom ratio.

Combined Hall effect,[31] electrical resistivity,[22] and specific heat measurements[23] tend to support the behavior suggested by the thermodynamic measurements. Comparison of these types of behavior with similar systems in which the tendencies toward ordering and clustering are independently measured indicate that:

1) At low temperatures, Cu-Zn alloys tend to order. This tendency increases with increasing zinc, to the solubility limit. At higher zinc concentrations, β brass shows an order-disorder transformation. As nickel is added to binary alloys, the tendency toward ordering decreases.

2) Cu-Ni alloys show a tendency toward clustering at somewhat higher temperatures, but still below the range of the diffusion anneals used in the present studies. This tendency diminishes as zinc is added to these binary alloys.

3) In the range of compositions near Cu_2NiZn a strong tendency toward ordering is observed, and some evidence supports the existence of long range order at low temperatures. In combination, these observations suggest that nickel atoms tend to cluster with each other, and zinc atoms tend to order with copper atoms. In the presence of a sufficient concentration of zinc, nickel atoms also tend to order with respect to copper.

In summary, size, electron concentrations, and thermodynamic effects tend to parallel one another in this

Table X. Diffusion Constants for Tracer Diffusion of Ni^{66} in Cu-Ni-Zn Alloys

Alloy Deisgnation	Composition, At. Pct Cu	Ni	Zn	Experimental Temperature Range, °C	Diffusion Constants[a] D^*_{0Zn}, cm^2/sec	Q^*_{Zn}, kcal/mole
00+	99.999	–	–	855-1055	$1.94^{+0.73}_{-0.50}$	55.6 ± 0.8
01+	90.25	–	9.75	791-995	$1.06^{+0.25}_{-0.16}$	52.3 ± 0.4
02+	80.08	–	19.92	777-946	$0.22^{+0.05}_{-0.04}$	46.6 ± 0.5
03+	70.94	–	29.06	739-895	$0.12^{+0.02}_{-0.02}$	43.2 ± 0.4
10+	90.08	9.92	–	929-1106	$0.31^{+0.09}_{-0.07}$	52.2 ± 0.6
11+	82.72	12.55	4.73	779-1027	$0.13^{+0.03}_{-0.02}$	49.6 ± 0.5
12+	72.04	11.21	16.75	784-999	$0.16^{+0.14}_{-0.13}$	47.8 ± 0.5
13+	65.06	10.82	24.12	794-959	$(8.44^{+1.80}_{-1.49})10^{-2}$	45.2 ± 0.5
20+	80.28	19.72	–	855-1097	$(6.36^{+4.77}_{-2.71})10^{-2}$	49.2 ± 1.4
21+	69.68	19.42	10.90	837-1041	$0.12^{+0.02}_{-0.02}$	49.7 ± 0.4
22+	63.95	20.80	15.25	837-1013	$(9.17^{+3.32}_{-2.43})10^{-2}$	48.2 ± 0.7
23+	55.17	20.59	24.24	791-983	$(9.90^{+3.20}_{-2.45})10^{-2}$	46.9 ± 0.7
30+	71.73	28.27	–	901-1134	$0.29^{+0.06}_{-0.05}$	54.2 ± 0.5
31+	60.97	29.49	9.54	904-1074	$0.42^{+0.11}_{-0.09}$	54.4 ± 0.6
32+	47.12	33.08	19.80	870-1050	$0.33^{+0.09}_{-0.07}$	52.8 ± 0.6
33+	40.30	30.70	29.00	885-995	$0.31^{+0.10}_{-0.09}$	51.6 ± 0.7

[a]Error limits refer to the probable error.

system. An equivalent statement appears to be that they are closely dependent upon each other. Thus, the arbitrary assignment of specific observations in the diffusion study to any one of these effects cannot be made unambiguously. Nonetheless, useful rationalizations of the interrelation between the diffusion study and the properties of solutions in the system may be made, and are presented in the following sections.

Variation of Diffusivity with Composition

The dependence of each of the three tracer diffusion coefficients upon composition at 900°C is shown in Figs. 7 to 9 and 12 to 14. In all three cases, the lines of constant diffusivity, Figs. 7 to 9, are roughly parallel to lines of constant electron concentration, molar volume, and activity coefficient for zinc. The high point of the diffusivity surfaces (on the binary Cu-Zn side) correspond to the high points on the molar volume and electron concentration surfaces: the low points (on the Cu-Ni binary) also correspond. Further, the diffusivities of the three species are in the order $D^*_{Zn}:D^*_{Cu}:D^*_{Ni}$, in the ratio 9:3:1.

The general increase in diffusivity of all three species as nickel is replaced by zinc may be rationalized as being attributed to an increase in the concentration of vacancies as the composition range is traversed

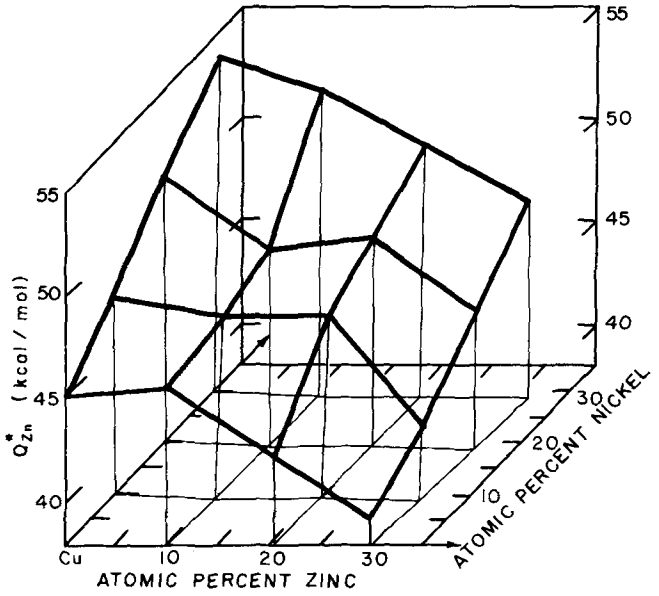

Fig. 30—Activation energy for diffusion of Zn^{65} in copper-rich Cu-Ni-Zn alloys.

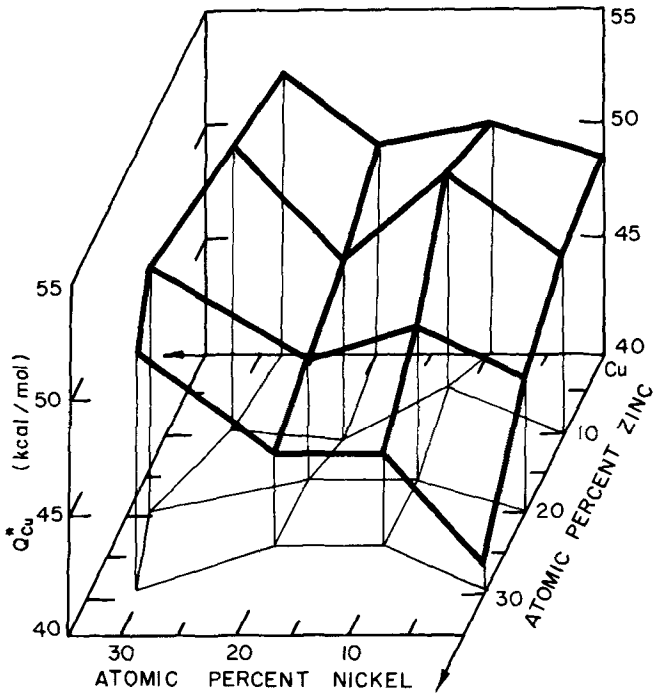

Fig. 31—Activation energy for diffusion of Cu^{67} in copper-rich Cu-Ni-Zn alloys.

from the 30 to the 03 alloys. The replacement of nickel with zinc exchanges a larger atom for a small one, and replaces an atom which contributes 0.6 electrons to the alloy with one that contributes 2 electrons. For tracer diffusion in very dilute solutions, it has been asserted that a large impurity atom tends to attract vacancies, because it compresses the surrounding lattice.[24] Also, an impurity which contributes a net number of electrons in the general cloud, and therefore has a net positive charge associated with the presence of its ion core, tends to attract vacancies, which would be expected to have a net negative charge.[25] Zinc appears to have both of these characteristics in the Cu-Ni-Zn system, while nickel is smaller than copper, and carries a net negative charge. Thus, both size

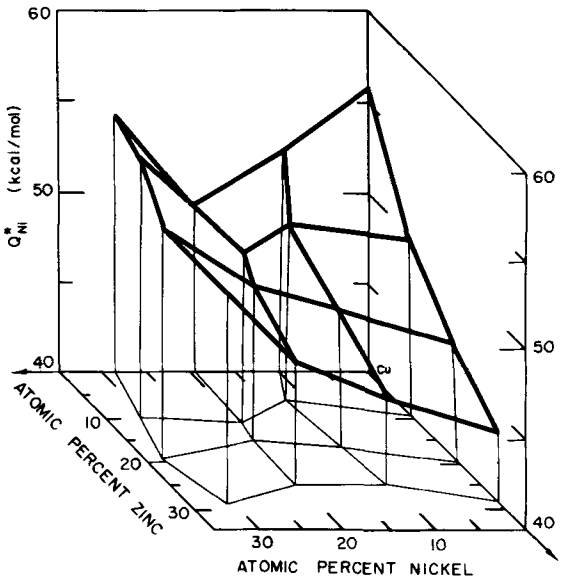

Fig. 32—Activation energy for diffusion of Ni^{66} in copper-rich Cu-Ni-Zn alloys.

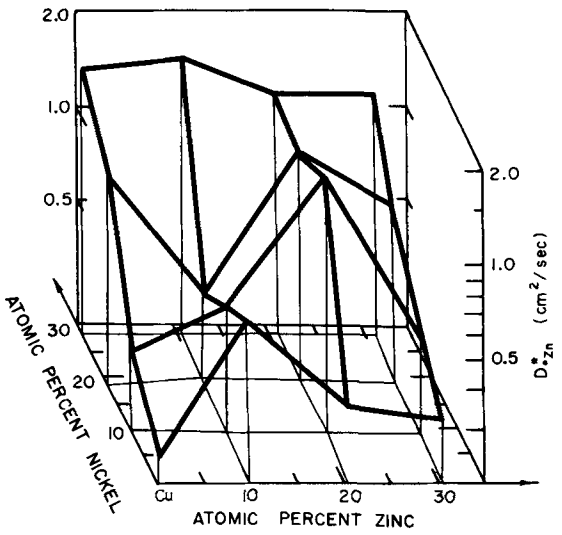

Fig. 33—Variation of the frequency factor, D^*_{0Zn}, with composition in the Cu-Ni-Zn system.

and electronic effects point to the preferential formation of vacancies around zinc atoms, and a rejection of vacancies in the vicinity of nickel atoms. As a result, the substitution of zinc for nickel as the concentration field is traversed from the 30 alloy to the 03 would qualitatively be expected to produce an increase in the general level of vacancy concentration, which would result in increased diffusivities for all three species, as is observed experimentally. Further, the vacancies present would tend to be associated with zinc atoms, and disassociated with from nickel atoms. This is consistent with the observed ordering of the relative magnitudes of the three diffusivities: $D^*_{Zn} > D^*_{Cu} > D^*_{Ni}$.

Variation of Activation Energies with Composition

Activation energies for diffusion, and preexponential (D^*_0) values are shown in Figs. 30 through 32 and 33

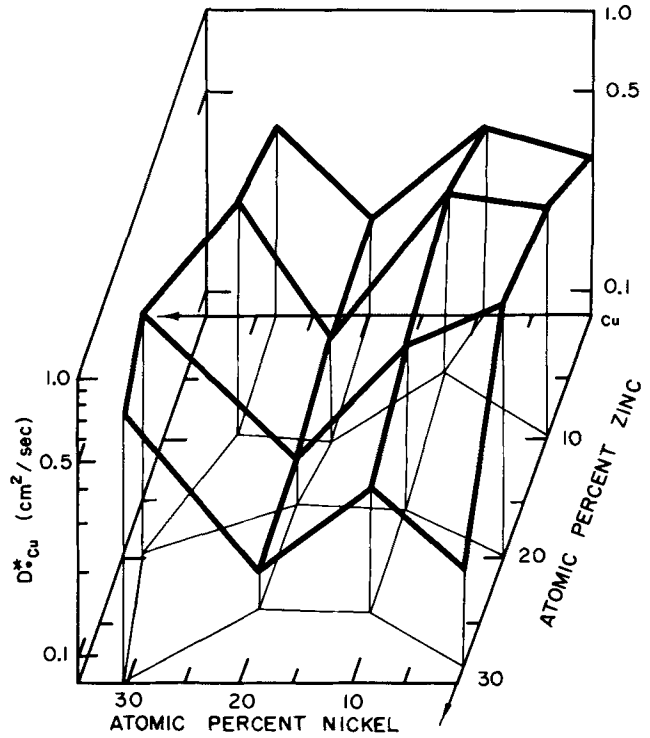

Fig. 34—Variation of the frequency factor, D^*_{0Cu}, with composition in the Cu-Ni-Zn system.

Table XI. Ratios of Diffusivities, Exponential Factors and D_0 Values for 03 and 30 Alloys

Tracer	Alloy	$D \times 10^{10}$, cm²/sec	Ratio	$e^{-Q/Rt} \times 10^{10}$	Ratio	D_0, cm²/sec	Ratio
Zn^{65}	03	158	127	470	590	0.32	0.23
	30	1.24		0.83	1.37	1.37	
Cu^{67}	03	49	31	91	109	0.12	0.41
	30	0.7		0.81		0.29	
Ni^{66}	03	9.9	70	280	150	0.16	0.47
	30	0.29		1.9		0.34	

through 35, respectively. Analysis of these figures shows that, at 900°C, for example, the composition dependence of the diffusion coefficients is primarily contained in the variation of the exponential factor, while the D^*_0 values are relatively composition insensitive. Table XI gives the ratios of D^* values, exponential factors and D^*_0 values at the 03 and 30 compositions. The ratio of D^* values is in the range from 30 to 127; that for the activation energies in the range from about 100 to 600. The D^*_0 ratios vary in the opposite direction with concentration, and the ratio ranges from about 1/4 to 1/2. Thus, most of the compositional variation in diffusivities results from compositional dependence of the activation energies.

The observation that the three activation energies are generally in the order $Q^*_{Ni} > Q^*_{Cu} > Q^*_{Zn}$ may be rationalized on the same basis as was the ordering of the diffusion coefficients. Both size and electron concentration effects are consistent with the hypothesis that the energy to form a vacancy is less near a zinc atom than it is near a nickel atom. Thus, the difference between activation energies, which averages about 2 kcal/mol between the activation energy surfaces for nickel and copper, and about 2 kcal/mol between those

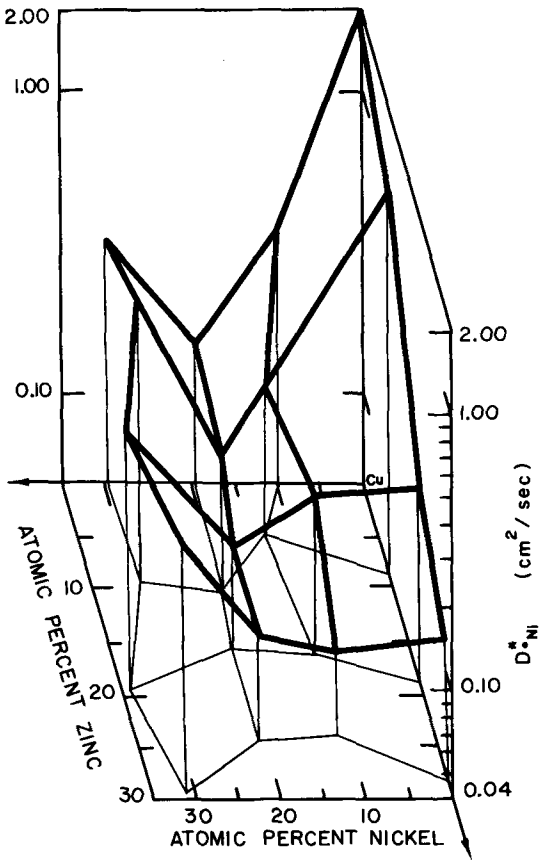

Fig. 35—Variation of the frequency factor, D^*_{0Ni}, with composition in the Cu-Ni-Zn system.

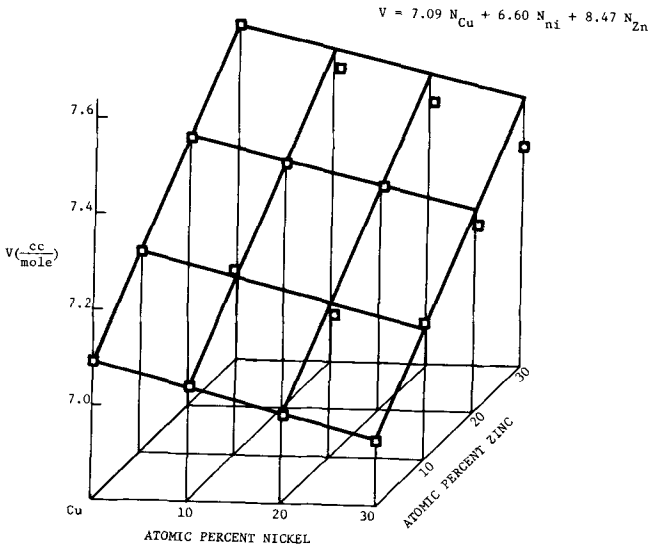

Fig. 36—Variation with composition of molar volume of Cu-Ni-Zn alloys.

for copper and zinc, would seem to be about the right order of magnitude for zinc-vacancy and nickel-vacancy interaction energies.

The rationale for the dependence of activation energies upon concentration is straightforward for the zinc tracer, but appears to be complicated for the copper and nickel tracers. Inspection of Fig. 30 shows that, for the diffusion of Zn^{65}, the activation energy is lowest for the 03 alloy, and highest for the 30 alloy. Isoactivation energy curves are roughly parallel to both lines of

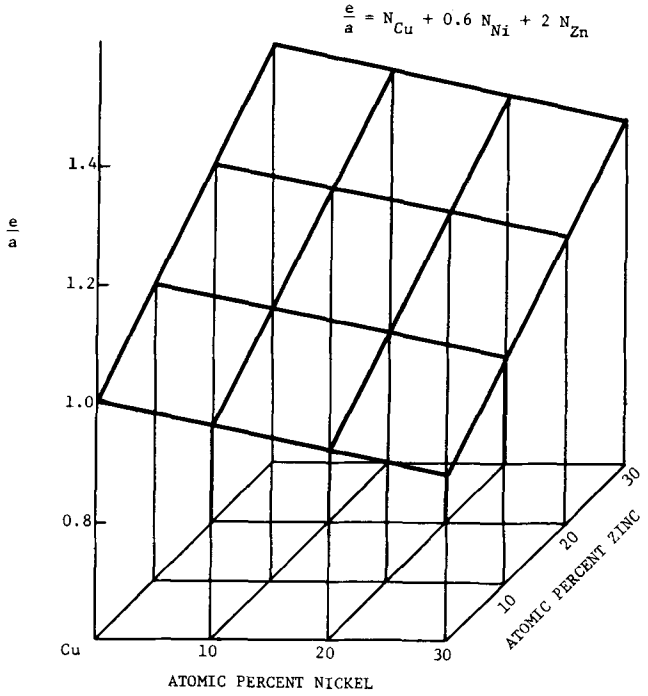

Fig. 37—Variation with composition of electron-to-atom ratio of Cu-Ni-Zn alloys.

constant molar volume and constant electron to atom ratio. Thus, the composition dependence of Q^*_{Zn} may be visualized as attributed to the composition dependence of the ease of creating vacancies near zinc atoms.

As the 03 corner of the composition range is approached, the surfaces for Q^*_{Cu} and Q^*_{Ni} behave essentially the same as that for zinc. Indeed, the three surfaces are roughly parallel, with the order of their stacking as described earlier. Along the copper-nickel binary, however, Q^*_{Ni} shows a definite minimum, which extends into the ternary composition range, and Q^*_{Cu} shows a relative minimum. In the range where these minima appear, both surfaces dip below that for Q^*_{Zn}.

This general behavior may be partially rationalized in terms of the clustering-ordering tendencies in the system described in an earlier section. On the basis of arguments already presented, zinc atoms tend to attract vacancies, and to avoid each other (*i.e.*, they tend to be ordered in the lattice). This combination of characteristics might be expected to tend to make the distribution of vacancies more homogeneous in the system as zinc is added. The compositional dependencies and relative magnitudes of the diffusivities and activation energies as the 03 corner is approached are consistent with this viewpoint. If, on the other hand, nickel atoms tend to cluster with each other, and to avoid vacancies, then along the Cu-Ni binary one might expect an inhomogeneous distribution of vacancies to result. The degree to which nickel atoms have access to the available vacancies would vary inversely with the degree to which these atoms cluster together. The minimum in activation energy that is observed along the Cu-Ni binary might be associated with a minimum in clustering tendency near the 20 composition. Such a postulate is completely speculative, however, since there is no evidence, either direct or indirect, supporting the existence or absence of such a minimum.

CONCLUSION

The diffusion behavior of the tracers Zn^{65}, Cu^{67}, and Ni^{66} in homogeneous ternary solid solutions of copper base Cu-Ni-Zn alloys has been determined experimentally in the composition range to 30 pct Zn and 30 pct Ni, and in the temperature range within 250°C of the solid-liquid envelope. It is found that:

1) The diffusivities of all three tracers decrease as nickel is added, and increase as zinc is added to pure copper. At 900°C, the diffusion coefficients of each specie increase by about 2 orders of magnitude as the composition range is traversed from 70 Cu-30 Ni to 70 Cu-30 Zn.

2) The diffusivities of the three tracers are consistently in the order: $D^*_{Zn} > D^*_{Cu} > D^*_{Ni}$. At 900°C, the ratio of the three diffusion coefficients is 9:3:1 over the entire composition range studied.

3) Along the Cu-Ni binary, the activation energies for the diffusion of both copper and nickel pass through a minimum at about 20 pct Ni. Otherwise, the activation energies of all three species increase as nickel is added and decrease as zinc is added to pure copper.

4) Except near the Cu-Ni binary, the activation energies for the three species are in the order: $Q^*_{Ni} > Q^*_{Cu} > Q^*_{Zn}$. Activation energies range from about 40 to 55 kcal/mol. The spacing between the activation energy surfaces over the composition plane is about 2 kcal/mol.

5) The composition dependence of the frequency factors, D^*_{oi}, tends to parallel that found for the activation energies.

6) Most of the variation in diffusivities with composition resides in the compositional dependence of the activation energies.

7) The compositional dependence of both the diffusivities and activation energies, as well as the relative magnitudes of the diffusivities and activation energies at any composition, are consistent with the relative sizes of the three atomic species in these alloys.

8) These dependencies are also consistent with the contribution of each specie to the electron to atom ratio in the system.

9) The minimum in activation energies for nickel and copper along the Cu-Ni binary may be associated with the tendency toward clustering in these alloys, but a satisfactory rationale for this effect could not be developed.

ACKNOWLEDGMENT

This work was supported, over a period of several years, by the Office of Naval Research, Contract No. NONR-580(13). The authors are grateful for this persevering support.

REFERENCES

1. L. S. Darken: *AIME Trans.*, 1948, vol. 175, p. 184.
2. J. S. Kirkaldy: *Can. J. of Phys.*, 1958, vol. 36, p. 899.
3. J. S. Kirkaldy and L. C. Brown: *Can. Met. Quart.*, 1963, vol. 2, p. 89.
4. J. R. Manning: *Phys. Rev.*, 1961, vol. 124, p. 470.
5. T. O. Ziebold and A. R. Cooper, Jr.: *Acta Met.*, 1965, vol. 13, p. 465.
6. R. T. DeHoff, A. G. Guy, K. J. Anusavice, and T. B. Lindemer: *Trans. TMS-AIME*, 1966, vol. 236, p. 881.
7. S. Yukama and M. J. Sinnott: *AIME Trans.*, 1955, vol. 203, p. 996.
8. B. Fisher and P. S. Rudman: *J. Appl. Phys.*, 1961, vol. 32, p. 1604.
9. H. P. Layer and R. O. Meyer: *Rev. Sci. Instrum.*, 1962, vol. 33, p. 1458.
10. K. J. Anusavice, J. J. Pinajian, H. Oikawa, and R. T. DeHoff: *Trans. TMS-AIME*, 1968, vol. 242, p. 2027.
11. A. G. Guy: University of Florida, private communication, 1969.
12. J. Crank: *The Mathematics of Diffusion*, Oxford University Press, London, 1956.
13. D. L. Styris and C. T. Tomizuka: *J. Appl. Phys.*, 1963, vol. 34, p. 1001.
14. A. J. Mortlock: *Trans. TMS-AIME*, 1968, vol. 242, p. 1963.
15. Computer Program BMDX 85: *Nonlinear Least Squares*, Paul Sampson, 1964, Health Sciences Computing Facility, Univ. of Calif., Los Angeles, Calif.
16. R. A. Swalin: *Thermodynamics of Solids*, John Wiley and Sons, Inc., New York, 1962.
17. R. A. Rapp and F. Maak: *Acta Met.*, 1962, vol. 10, p. 63.
18. W. Hume-Rothery and C. W. Howarth: *Phil. Mag.*, 1954, vol. 43, p. 613.
19. G. A. Chadwick and B. B. Argent: *Trans. Faraday Soc.*, 1961, vol. 57, p. 2138.
20. G. A. Chadwick and B. B. Argent: *J. Inst. Metals*, 1959, vol. 88, p. 318.
21. W. Koster: *Metall.*, 1960, vol. 7, p. 641.
22. W. Koster and E. W. Schule: *Z. Metallk.*, 1957, vol. 48, p. 595.
23. D. R. Kussmann and C. E. Wollenberger: *Naturwiss.*, 1956, vol. 43, p. 395.
24. P. G. Shewmon: *Diffusion in Solids*, McGraw-Hill Book Co., Inc., New York, 1965.
25. A. D. LeClaire: *Phil. Mag.*, 1962, vol. 7, p. 141.